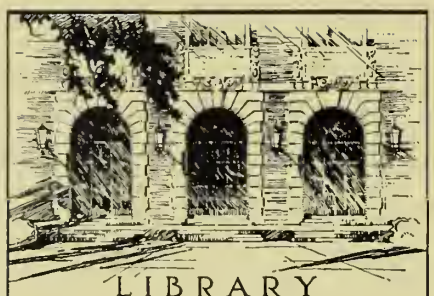

Antenna Laboratory
Technical Report No. 10

AN ANALYTICAL STUDY
of
SPACED LOOP ADF ANTENNA SYSTEMS

Contract No. AF33(616)-3220
Project No. 6(7-4600)Task 40572
WRIGHT AIR DEVELOPMENT CENTER

by

D. G. Berry
and
J. B. Kreer

10 May 1956

Electrical Engineering Research Laboratory
Engineering Experiment Station
University of Illinois
Urbana, Illinois

ABSTRACT

The patterns of three multiple loop antenna systems (including a goniometer) are investigated analytically to determine whether these systems offer an improvement in polarization and reradiation error over a single loop when mounted on a long conducting cylinder with a circumference of approximately one-half wavelength. Goniometer patterns are presented and are summarized by plots of indicated versus actual direction of arrival. The four-element spaced loop system with all of the loop axes oriented in the direction of the cylinder axis is the most promising, since the polarization error is comparatively small. The four loop system with loop axes in the circumferential direction and a system with loops above and below the cylinder proved to have quite large polarization and reradiation errors. The results, and particularly the negative results, may be extended qualitatively to these antenna systems when mounted on missiles and aircraft.

CONTENTS

ILLUSTRATIONS

ACKNOWLEDGMENT

The spaced loop systems described in this report were originally proposed by Drs. E. C. Jordan, A. D. Bailey, and R. C. Hansen. Prof. V. H. Rumsey suggested that a theoretical investigation be made of these systems when placed on an infinitely long cylinder. Dr. R. H. DuHamel was the supervisor of the work.

1. INTRODUCTION

The development of an antenna system for use in radio direction finding in the 3-18 mc frequency range is made necessary by the severe limitations that are inherent in the ordinary rotatable loop antenna in this range. The single loop, whether mounted on an aircraft or in free space, introduces an error in the RDF system whenever the exciting wave is not incident from the horizon. This error is due to the voltage induced by the horizontally polarized portion of the field. Because ionospherically reflected waves are common in this frequency range, this polarization error is a serious enough defect to make the single loop unusable for airborne RDF. Another error arises from the fact that the longest portions of modern aircraft are long enough to be appreciable portions of a wavelength in the 3-18 mc range. Because of this, large currents are induced in the wings, fuselage, etc., by an incident wave. The fields reradiated from these currents induce voltages in the loop antenna which are not simply related to the direction of arrival of the incident field and, therefore, cause further error to be introduced into the system.

The approach taken in an attempt to devise an antenna system which would provide reliable RDF information in the frequency range under consideration was to space a number of fixed, flush mounted, suitably interconnected, loop antennas about the aircraft. Although this idea is not new, recent work with ferrite cores indicates that it is now possible to get sensitivity adequate for RDF work from flush mounted loops. Flush mounting is, of course, essential on high speed aircraft.

That a system of spaced loops would give an improvement in polarization error is suggested by the fact that two loops closely spaced in free space, connected in phase opposition and oriented so that they are either coaxial or coplaner, are free of polarization error. That is, the pattern of the loops maintains two of its nulls in the same position regardless of the polarization of the incident field.

2. SPACED LOOP SYSTEMS UNDER CONSIDERATION

Two specific multiple loop systems have been under investigation. The first, which is illustrated in Figure 1, consists of one pair of coaxial loops and one pair of coplaner loops, closely spaced and mounted so that each loop is located at a corner of a square. Both coaxial and coplaner loops are connected out of phase. The outputs of each pair are fed through a sine, cosine goniometer. The goniometer output from this system, which is derived in Appendix I, is seen to be (for a given polarization and direction of arrival of the incident wave) proportional to sin $(\phi-\gamma)$ when the loops are mounted in free space, where ϕ is the azimuthal angle of arrival and γ is the goniometer angle. The goniometer output then is a "figure eight" pattern, independent of the polar angle of arrival and the polarization angle, which has its nulls in the direction of arrival (ϕ) and 180° from that direction. To insure sensitivity in all directions, two of these systems could be mounted at right angles and the one with maximum output used.

The second system that was investigated, which is illustrated in Fig. 2, also uses four loops and a goniometer. In this case, one loop is mounted on top of a wing, fuselage, etc. and another loop which is coplaner with it is mounted below. These two loops are connected so that voltages induced in them by the incident wave add in phase. At right angles to this pair is another pair of loops similarly connected. As in the system previously described, the loop pairs are fed through a goniometer to some indicating device. This system was chosen for investigation because the balanced loop arrangement has been shown[1] to offer improvement in reradiation error for waves incident from near the horizon.

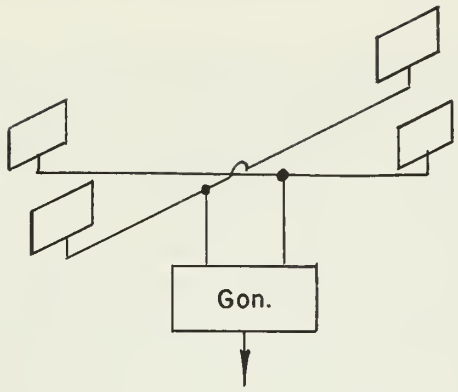

Figure 1. Illustration of a Multiple Loop System having Opposite Loops Connected Out of Phase and Fed Through a Sine, Cosine Goniometer

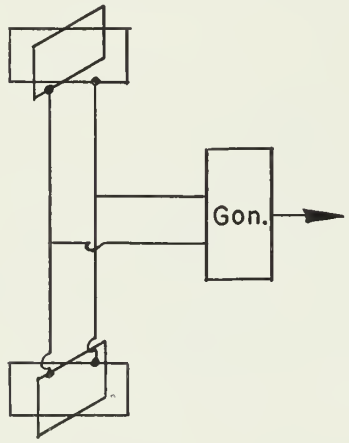

Figure 2. A Spaced Loop-Goniometer System Having Loops Mounted Above and Below a Wing, Fuselage, etc.

3. METHODS OF ANALYSIS

In order to see whether these multiple loop systems held promise for airborne RDF use, the behavior of the goniometer pattern was investigated analytically when the loops were mounted on a conducting body of simple geometry. The idea was that if the multiple loop system showed marked improvement in reradiation and polarization error when mounted near a conducting body of simple geometry (in this case a right circular cylinder with a scattered field which could be easily investigated*), then it would probably prove worthwhile to investigate by experimental methods the behavior of the system when mounted on an aircraft.

The method used to calculate the goniometer pattern is as follows: A plane wave, linearly polarized, is assumed to impinge, from an arbitrary direction, on an infinitely long, perfectly conducting cylinder. The total field outside of the cylinder is then the sum of the incident wave and the scattered field. The voltage induced in a small loop immersed in the total field is proportional to the component of magnetic field that is normal to the plane of the loop. For all of the cases considered the loops were assumed to be mounted at the surface of this cylinder. The details of the mathematics are summarized in Appendix II.

Figures 3, 4, and 5 illustrate the orientation of the conducting cylinder with respect to the coordinate system used in the calculations and the orientation of the loops on the cylinder. The four-loop system illustrated in Fig. 1 was investigated in two positions with respect to the cylinder. Figure 3 illustrates this system oriented with its loop axes in the circumferential direction of the cylinder, whereas Fig. 4 shows this system with its loop axes in the axial direction of the cylinder. In each case, loops one and two are connected in phase opposition as are loops three and four. The output of each pair is fed into one input of a goniometer.

The loop system illustrated in Fig. 2 is shown mounted on the cylinder in Fig. 5. Loops one and two are connected so that the voltages induced in them by the incident field will add and are fed through a goniometer, as are loops three and four.

---

* The system of calculating the patterns of small antennas when mounted on a perfectly conducting, infinitely long, right circular cylinder was developed by Carter.[2] It was later put in a more usable form and extended to elliptical cylinders by Sinclair.[3]

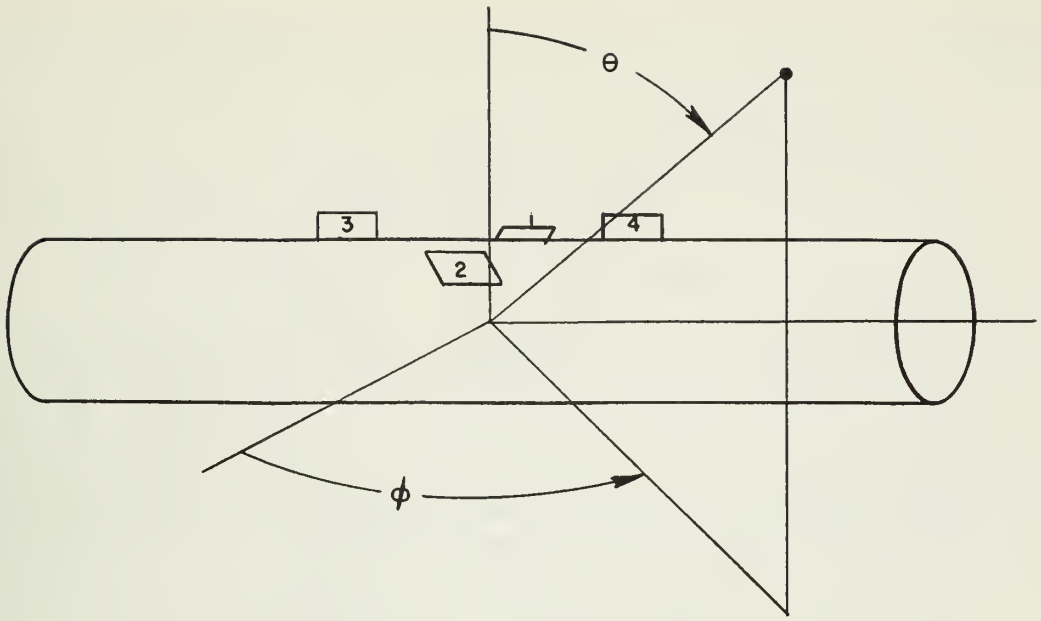

Figure 3. The Four Loop System of Figure One Mounted on a Cylinder with the Loop Axes in the Circumferential Direction of the Cylinder

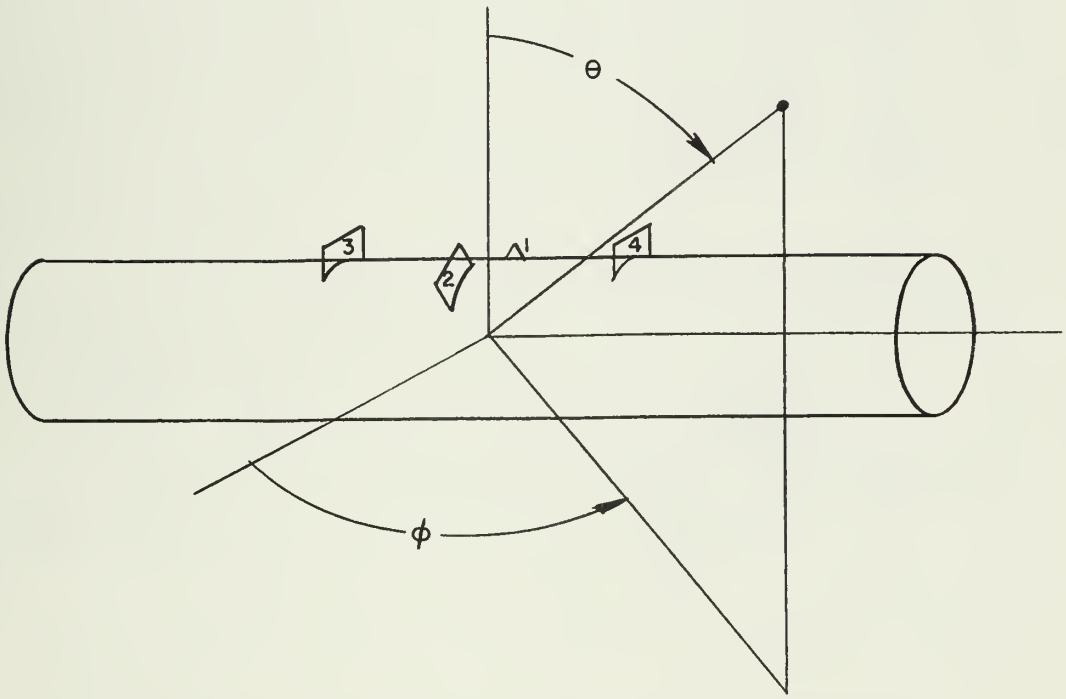

Figure 4. The Four Loop System of Figure One Mounted on a Cylinder with the Loop Axes in the Axial Direction of the Cylinder

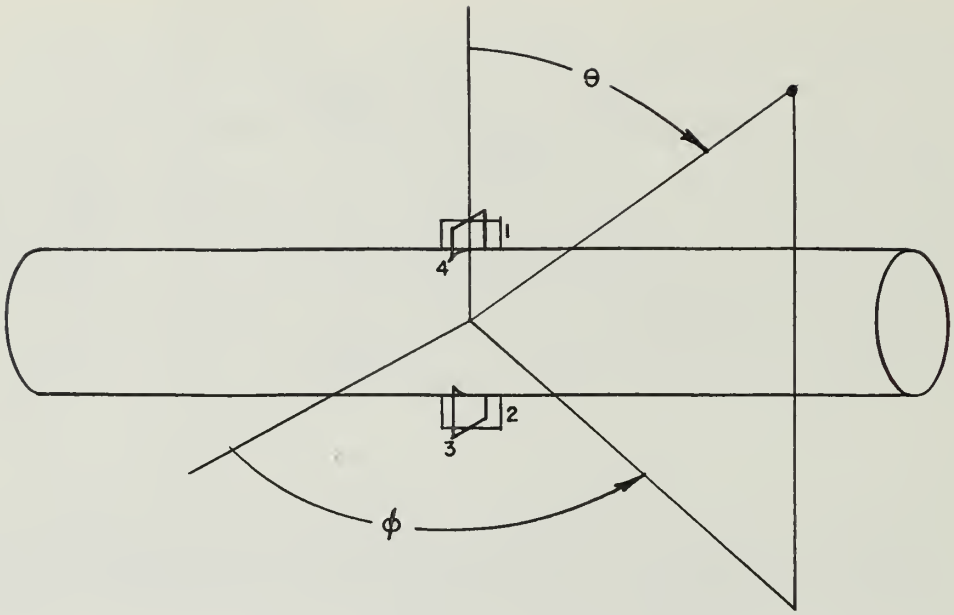

Figure 5. The Loop System of Figure 2 Mounted on a Cylinder

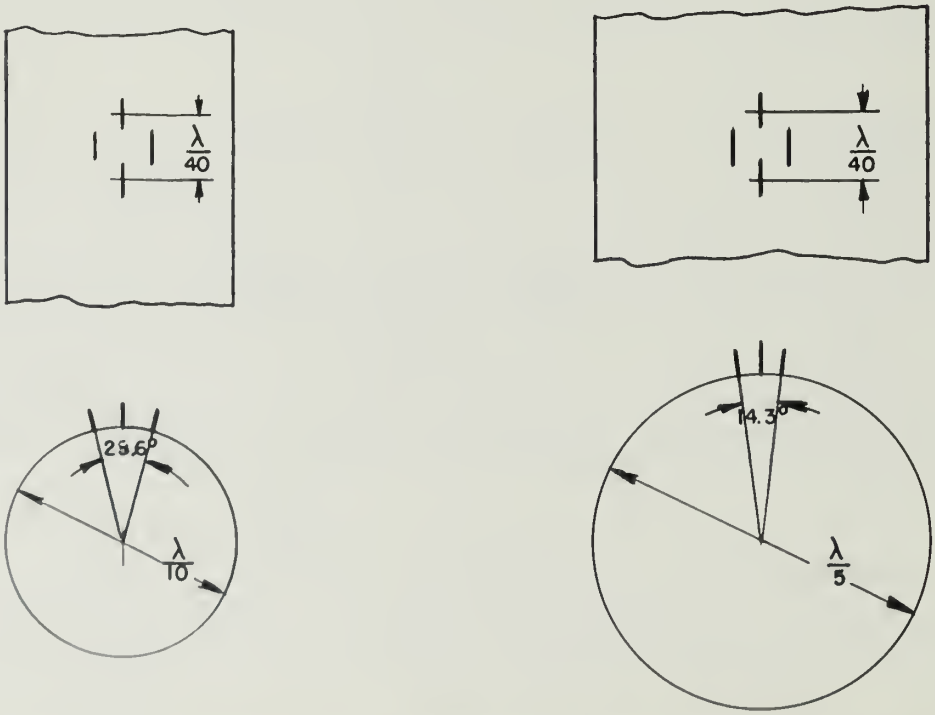

Figure 6. The Positions of the Loops When Mounted on Cylinders of Diameter λ/10 and λ/5

Figure 6 illustrates the cylinder size and the spacing of the loops used in the calculations. One set of data was calculated using a cylinder with a diameter of $\lambda/10$ and a loop spacing (between members of a pair) of $\lambda/40$. Another set was taken for a cylinder with a diameter twice as large but with the same loop spacing.

The data were calculated in the following manner. The incident wave was assumed to be polarized in the θ direction and arriving from the direction defined by $\theta = 80^{o}$, $\phi = 0^{o}$. With the incident field as described and the goniometer connected to the output of the two sets of loops under consideration the goniometer was rotated (mathematically in ten degree increments) through 360^{o}. If the loops were mounted in free space this pattern of the goniometer would be $\sin(\phi-\gamma)$, γ being the goniometer angle. Next, the incident wave was set to arrive from $\theta = 80^{o}$, $\phi = 10^{o}$ and the goniometer process repeated. This was repeated in 10^{o} increments through $\phi = 90^{o}$. These results are illustrated in the (a) parts of Figs. 7 through 15.

Next, a wave having the same polarization was assumed to come from the direction defined by $\theta = 45^{o}$, $\phi = 0^{o}$ Goniometer patterns were again calculated in 10^{o} (ϕ) increments. These results are shown in the (b) parts of Figs. 7 through 15.

This entire set of patterns was then calculated for an incident wave having 45^{o} polarization, i.e., polarization that has equal θ and ϕ components. These results are shown in the (c) and (d) parts of Figs. 7 through 15. The complete set of patterns is shown for the system illustrated in Fig. 3. The patterns of the other systems are shown only in part.

Figures 16, 21, and 26 summarize the information obtained from the goniometer patterns. Each figure is a plot of indicated bearing (position of minimum goniometer reading) versus actual bearing (azimuthal direction of wave arrival) for all sets of goniometer patterns calculated. These curves indicate the susceptibility of these systems to error due to the presence of horizontally polarized and reradiated fields.

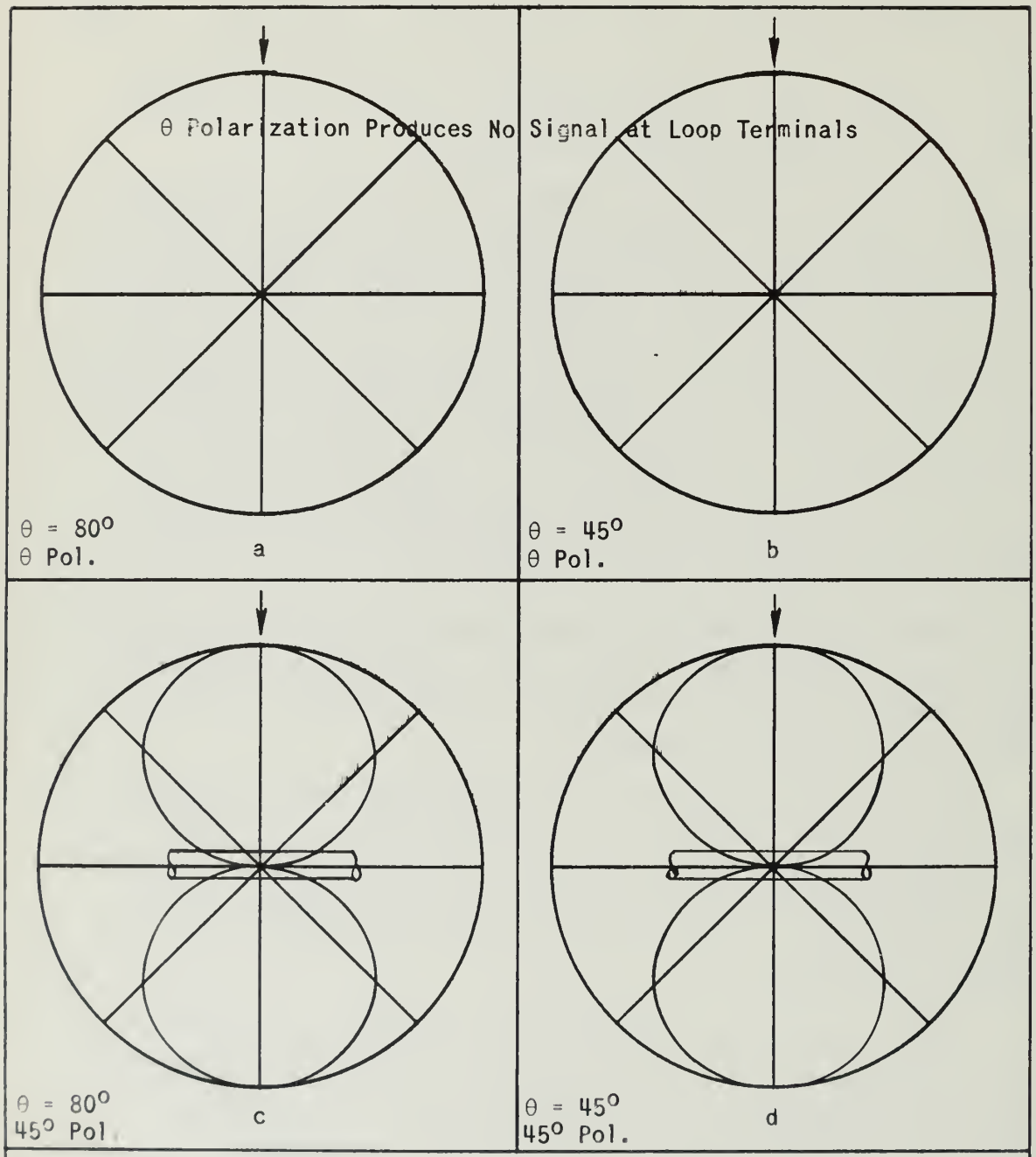

Figure 7. Goniometer Patterns of the Four Loop System Mounted on a Conducting Cylinder of Diameter $\lambda/10$ with the Loop Axes in the Circumferential Direction of the Cylinder and the Exciting Wave Incident from $\phi = 0^{\circ}$

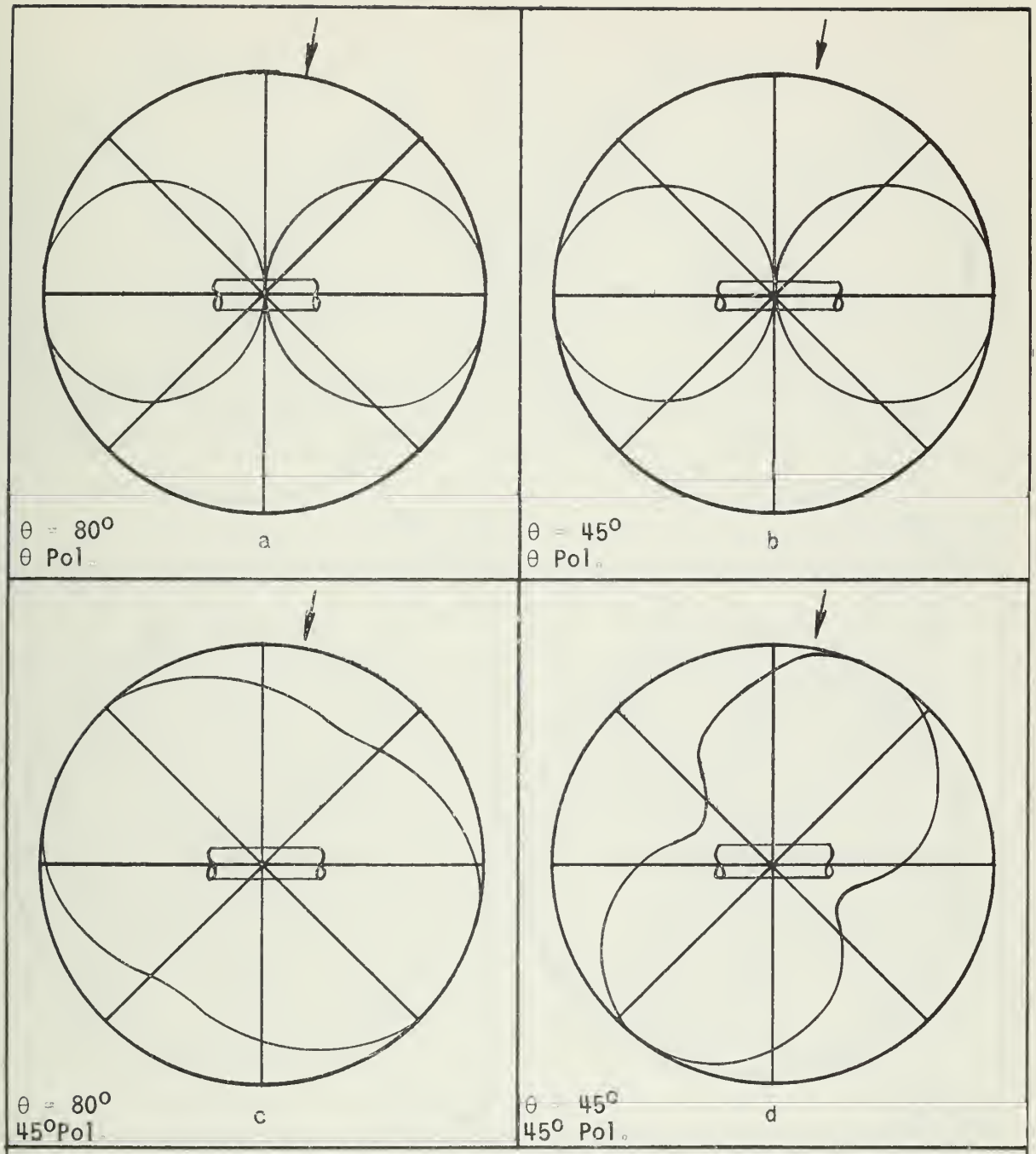

Figure 8. Goniometer Patterns of the Four Loop System Mounted on a Conducting Cylinder of Diameter $\lambda/10$ with the Loop Axes in the Circumferential Direction of the Cylinder and the Exciting Wave Incident from $\phi = 10^{\circ}$

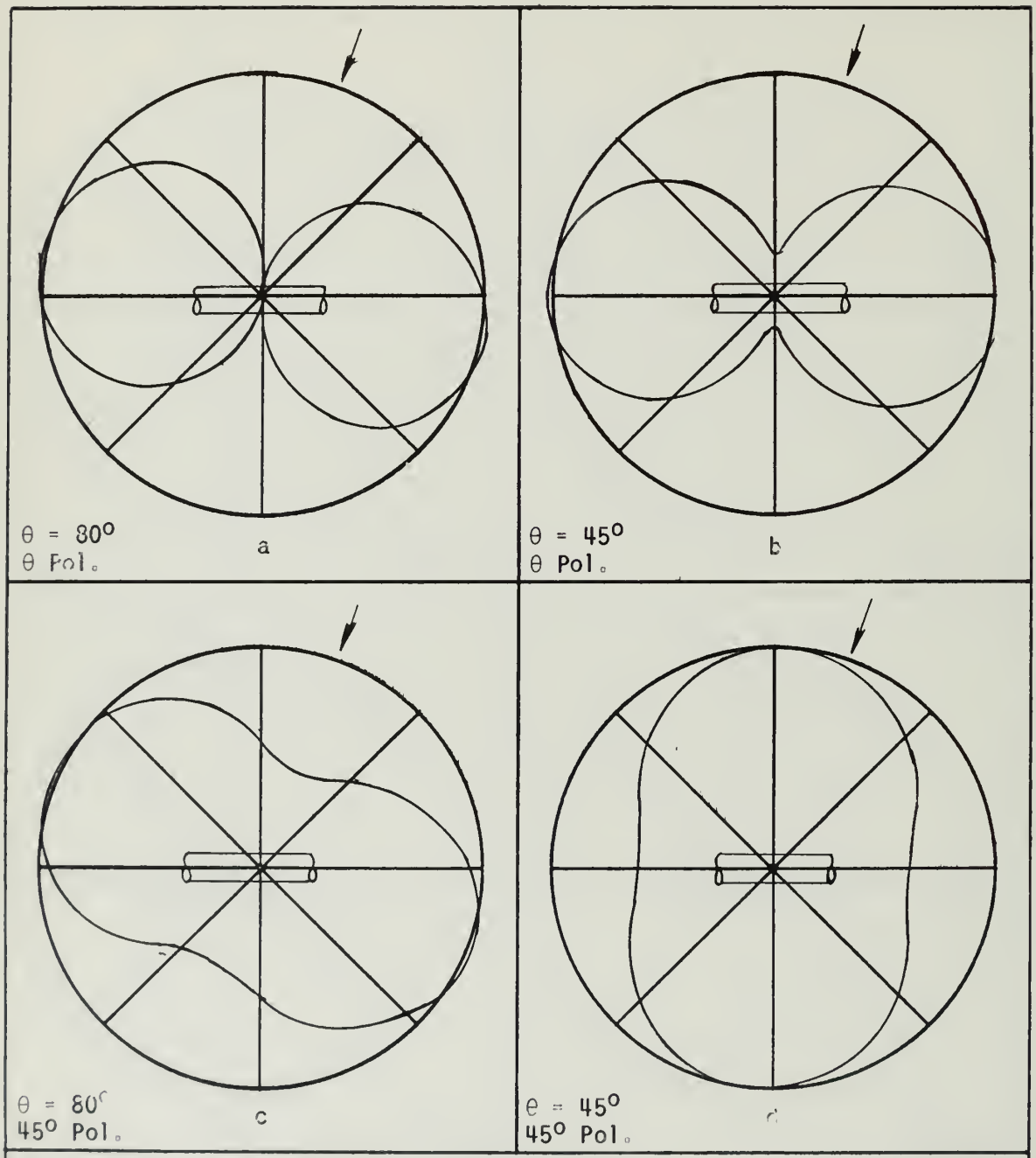

Figure 9. Goniometer Patterns of the Four Loop System Mounted on a Conducting Cylinder of Diameter λ/10 with the Loop Axes in the Circumferential Direction of the Cylinder and the Exciting Wave Incident from $\phi = 20^{\circ}$

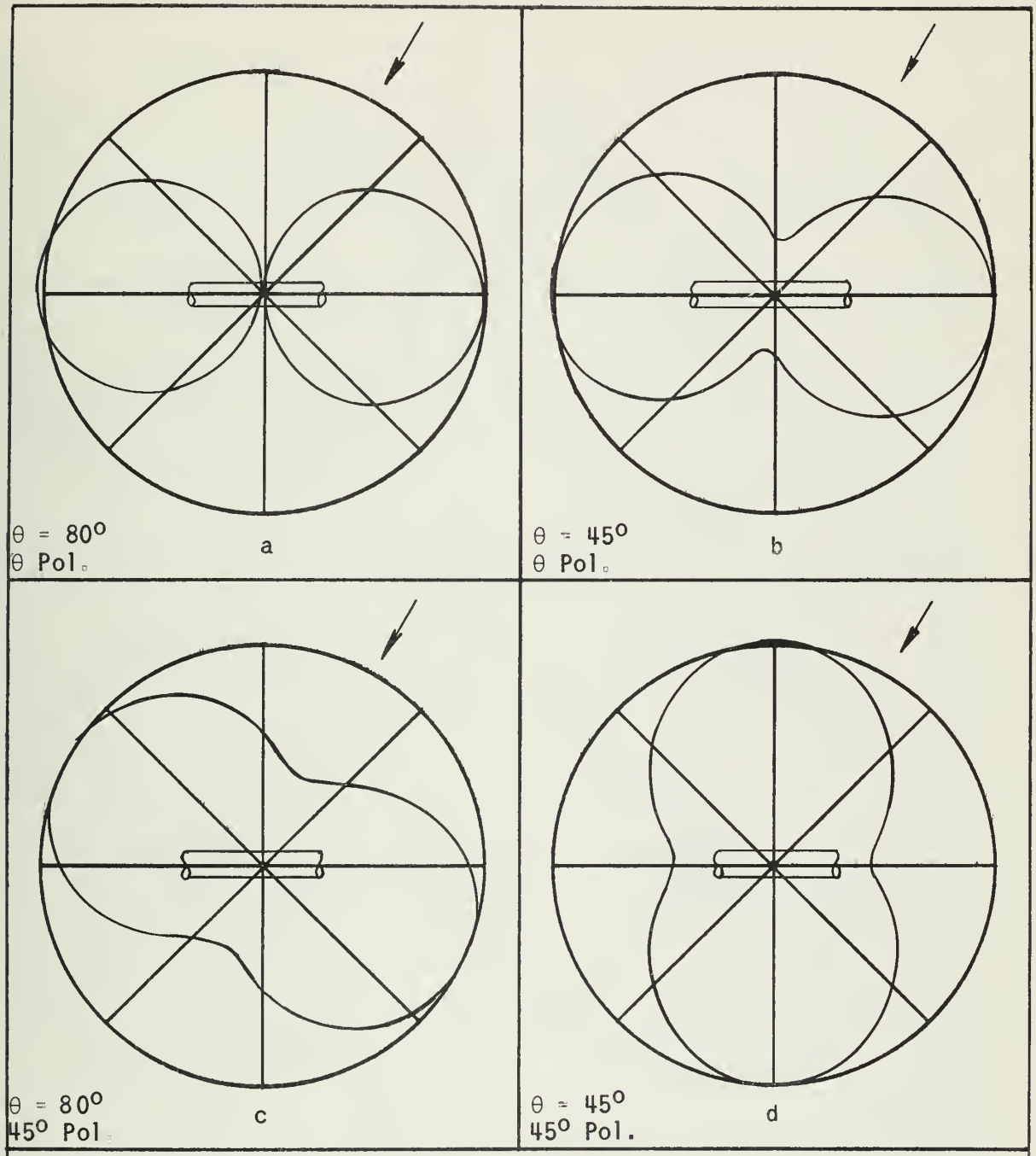

Figure 10. Goniometer Patterns of the Four Loop System Mounted on a Conducting Cylinder of Diameter $\lambda/10$ with the Loop Axes in the Circumferential Direction of the Cylinder and the Exciting Wave Incident from $\phi = 30^{\circ}$

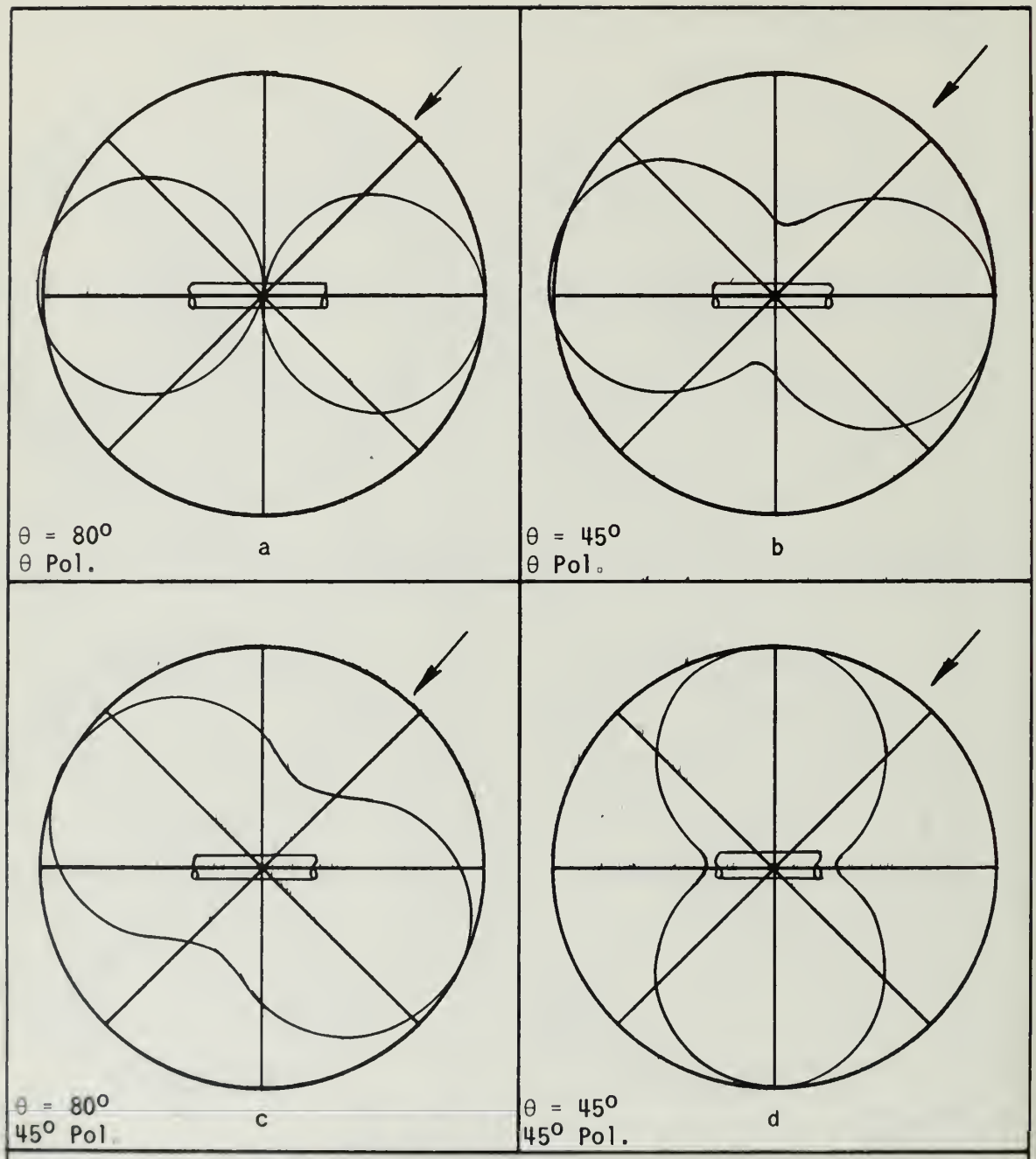

Figure 11. Goniometer Patterns of the Four Loop System Mounted on a Conducting Cylinder of Diameter $\lambda/10$ with the Loop Axes in the Circumferential Direction of the Cylinder and the Exciting Wave Incident from $\phi = 40^{\circ}$

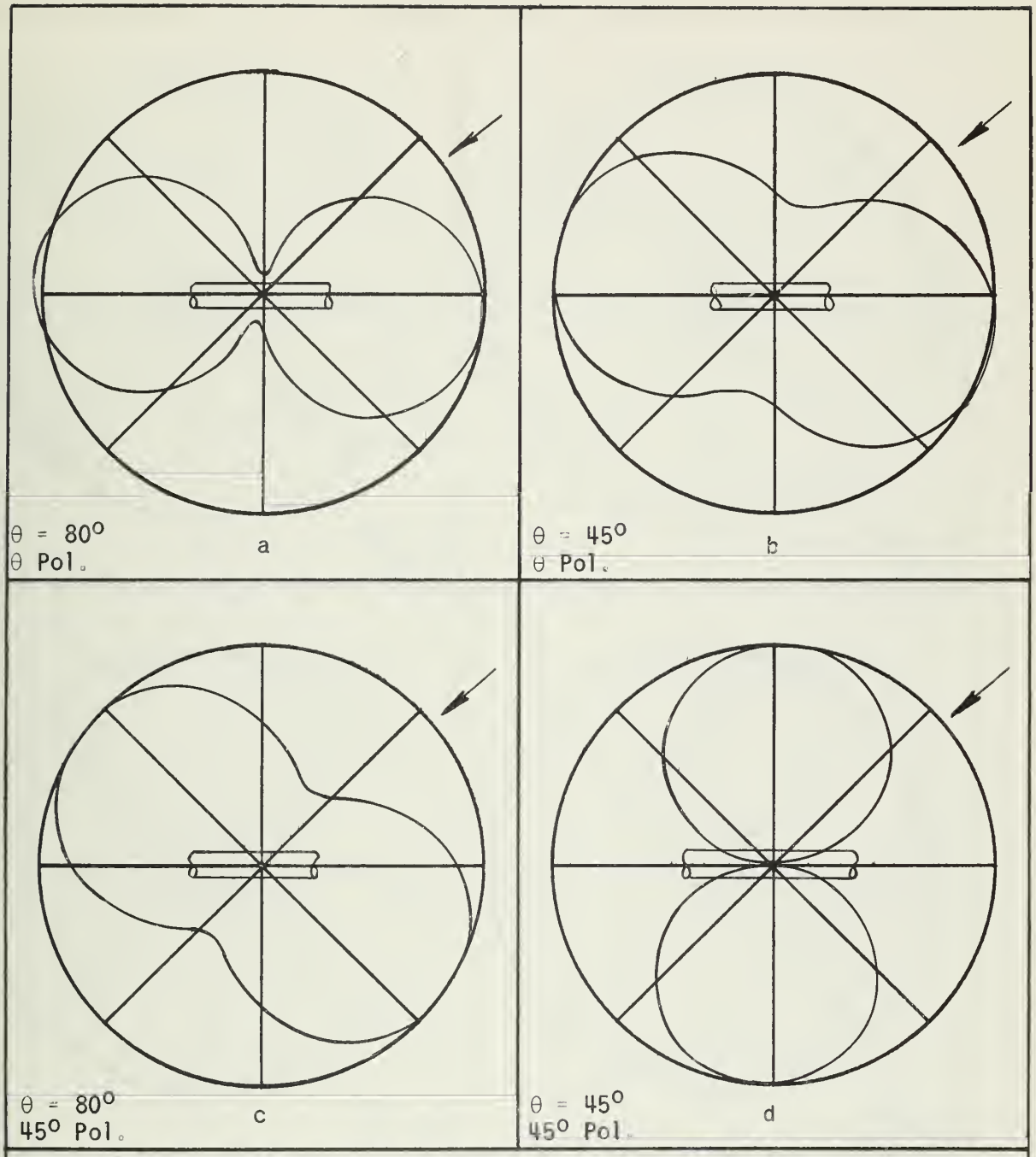

Figure 12. Goniometer Patterns of the Four Loop System Mounted on a Conducting Cylinder of Diameter $\lambda/10$ with the Loop Axes in the Circumferential Direction of the Cylinder and the Exciting Wave Incident from $\phi = 50^{\circ}$

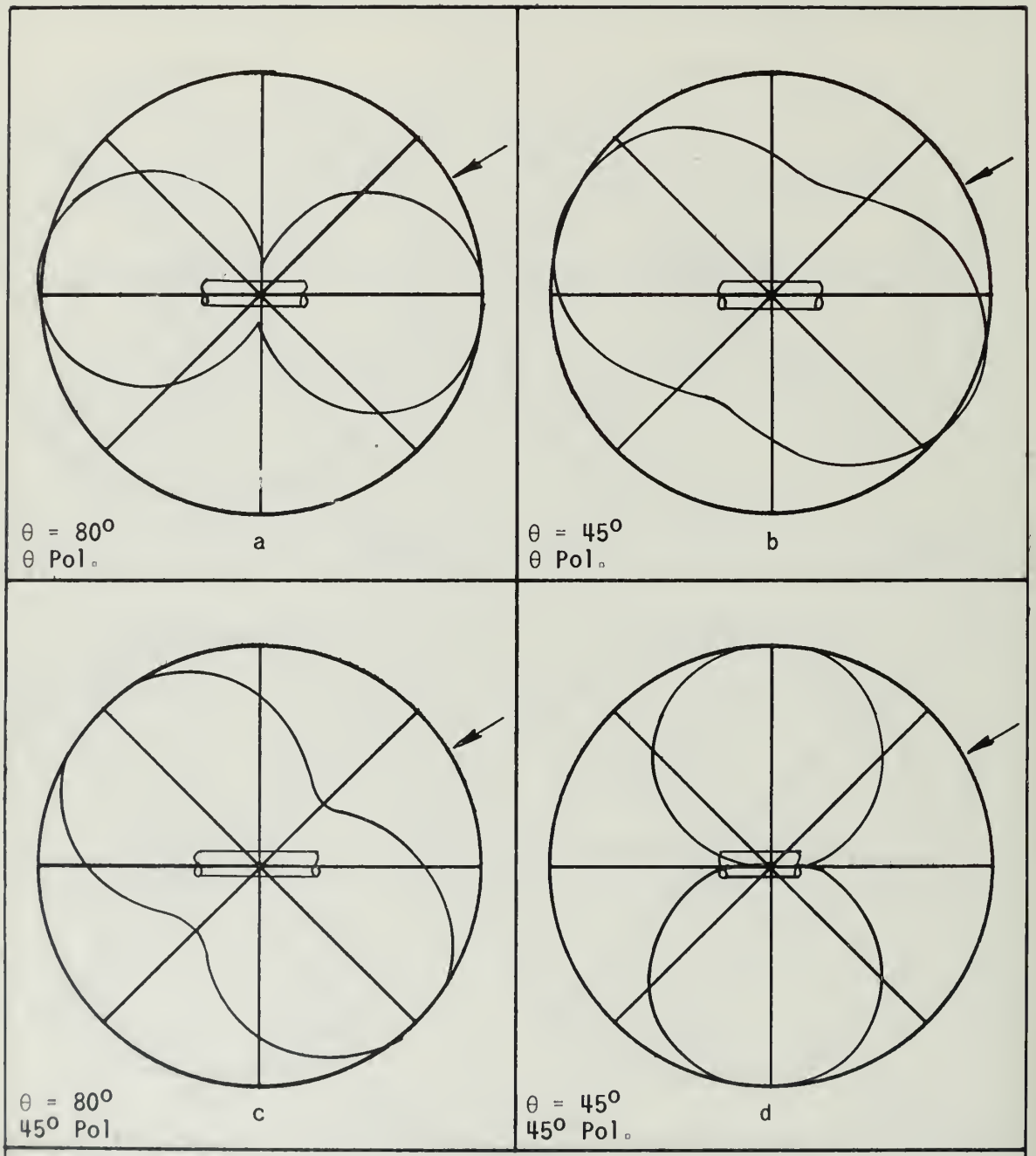

Figure 13. Goniometer Patterns of the Four Loop System Mounted on a Conducting Cylinder of Diameter $\lambda/10$ with the Loop Axes in the Circumferential Direction of the Cylinder and the Exciting Wave Incident from $\phi = 60^{\circ}$

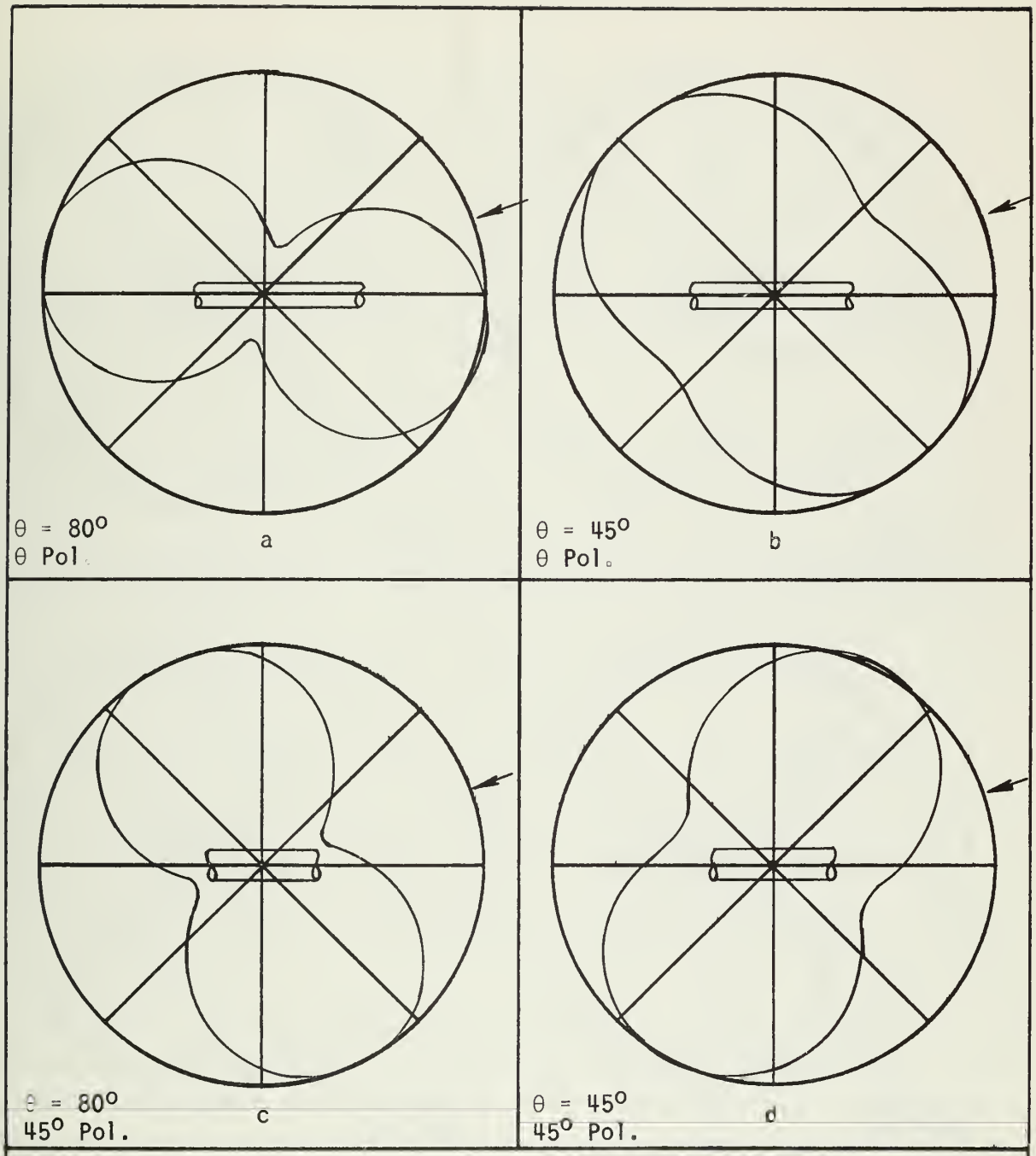

Figure 14. Goniometer Patterns of the Four Loop System Mounted on a Conducting Cylinder of Diameter $\lambda/10$ with the Loop Axes in the Circumferential Direction of the Cylinder and the Exciting Wave Incident from $\phi = 70^{\circ}$

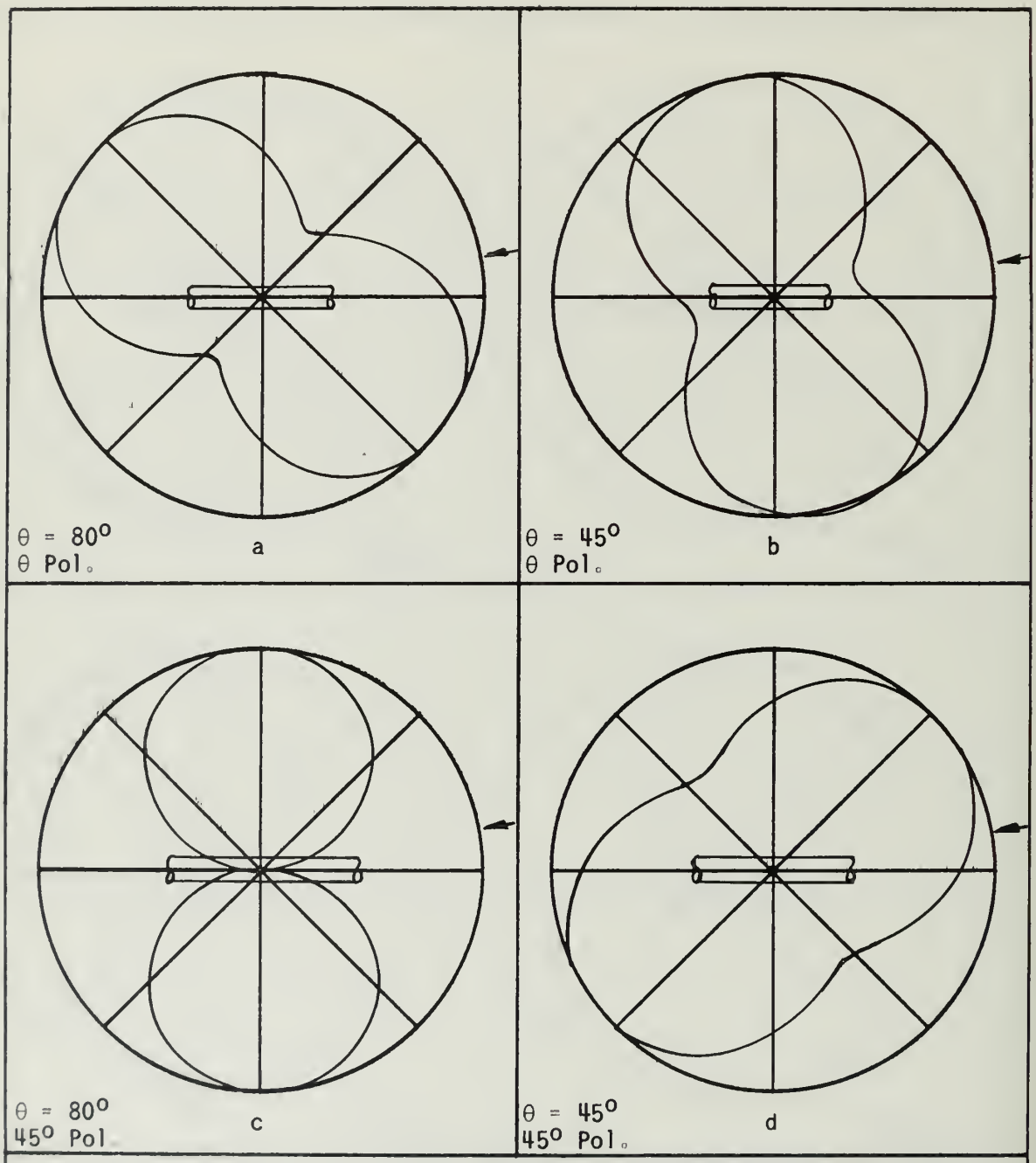

Figure 15. Goniometer Patterns of the Four Loop System Mounted on a Conducting Cylinder of Diameter $\lambda/10$ with the Loop Axes in the Circumferential Direction of the Cylinder and the Exciting Wave Incident from $\phi = 80^{\circ}$

4. ANALYSIS OF RESULTS

Figures 7 through 15 show the goniometer patterns of the spaced loop system of Fig. 3 mounted on a cylinder of diameter equal to $\lambda/10$. These were calculated for values of ϕ in 10^{o} steps from 0^{o} to 80^{o} and for $\theta = 80^{o}$ and $\theta = 45^{o}$ for both 0^{o} and 45^{o} polarization. It can be seen that the shape of these patterns (and hence the information derived from them) is not dependent on ϕ alone as is desired but varies greatly with elevation and polarization angles of the incident field. Figure 16, which is a plot of null position versus the azimuthal angle of incidence, points this up quite clearly.

The same can be said of Figs. 17 through 20 although the effect of polarization is much less pronounced. These figures are the goniometer patterns of the spaced loop system of Fig. 4 mounted on a cylinder of diameter equal to $\lambda/10$. These patterns were calculated for the same values of ϕ, θ and polarization angles as the previous set, but only the patterns calculated for fields incident from $\phi = 10^{o}$, 30^{o}, 50^{o}, and 70^{o} are shown here. Figure 21 is the plot of true versus indicated bearing for this antenna system.

Figures 22 through 25 are the goniometer patterns of the antenna system illustrated in Fig. 5. These were calculated for the same parameters as the previous systems but again only the patterns calculated for fields incident from $\phi = 10^{o}$, 30^{o}, 50^{o}, and 70^{o} are presented. The patterns of this antenna system are also affected by elevation angle and, to a very great degree, by polarization angle, as shown in Fig. 26.

The above comments are, in general, applicable to Figs. 27, 28, and 29 which are the goniometer patterns of the same antenna systems as above when mounted on a cylinder of diameter equal to $\lambda/5$.

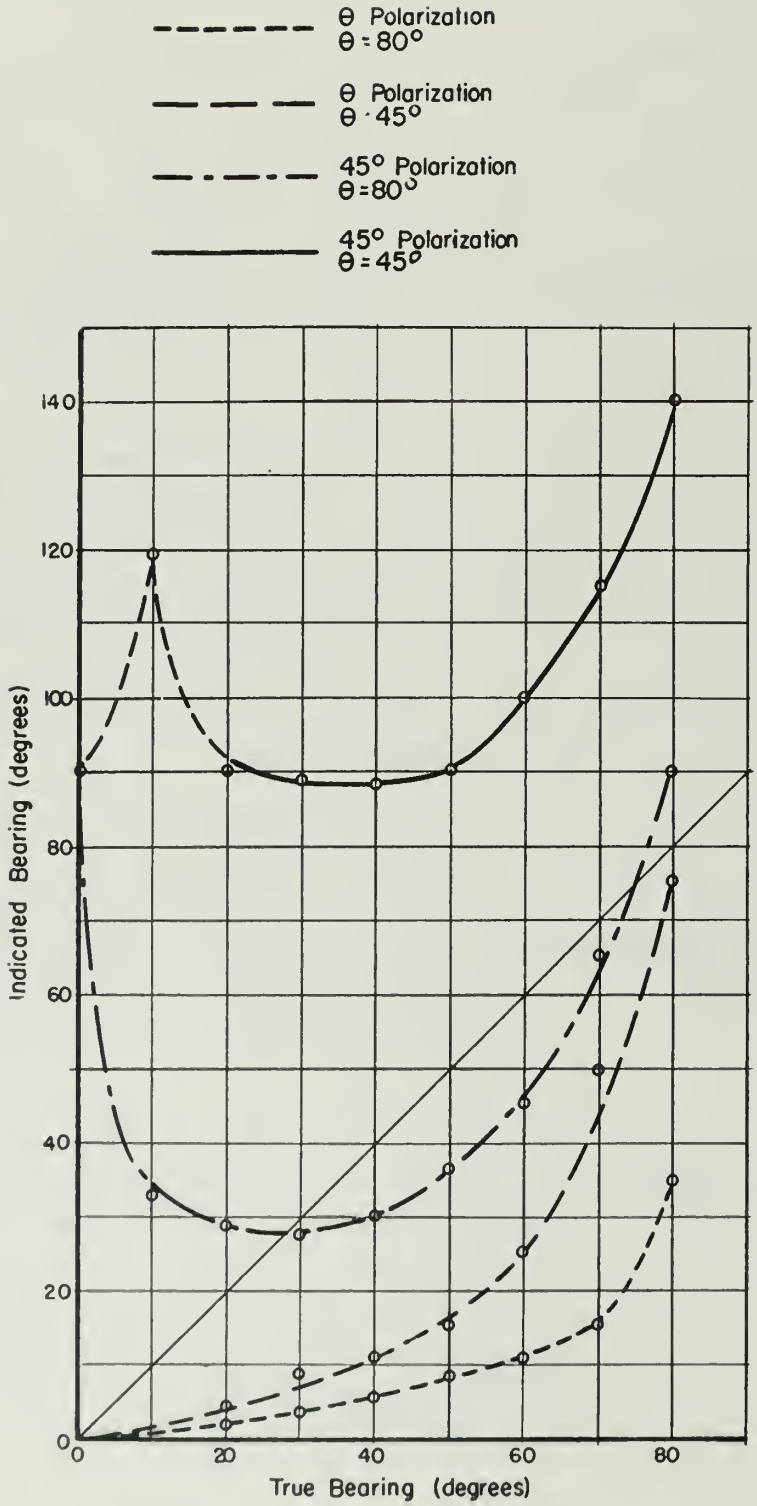

Figure 16 True Bearing versus Indicated Bearing for the Four Loop System Mounted on a Long Cylinder (Axes Circumferential)

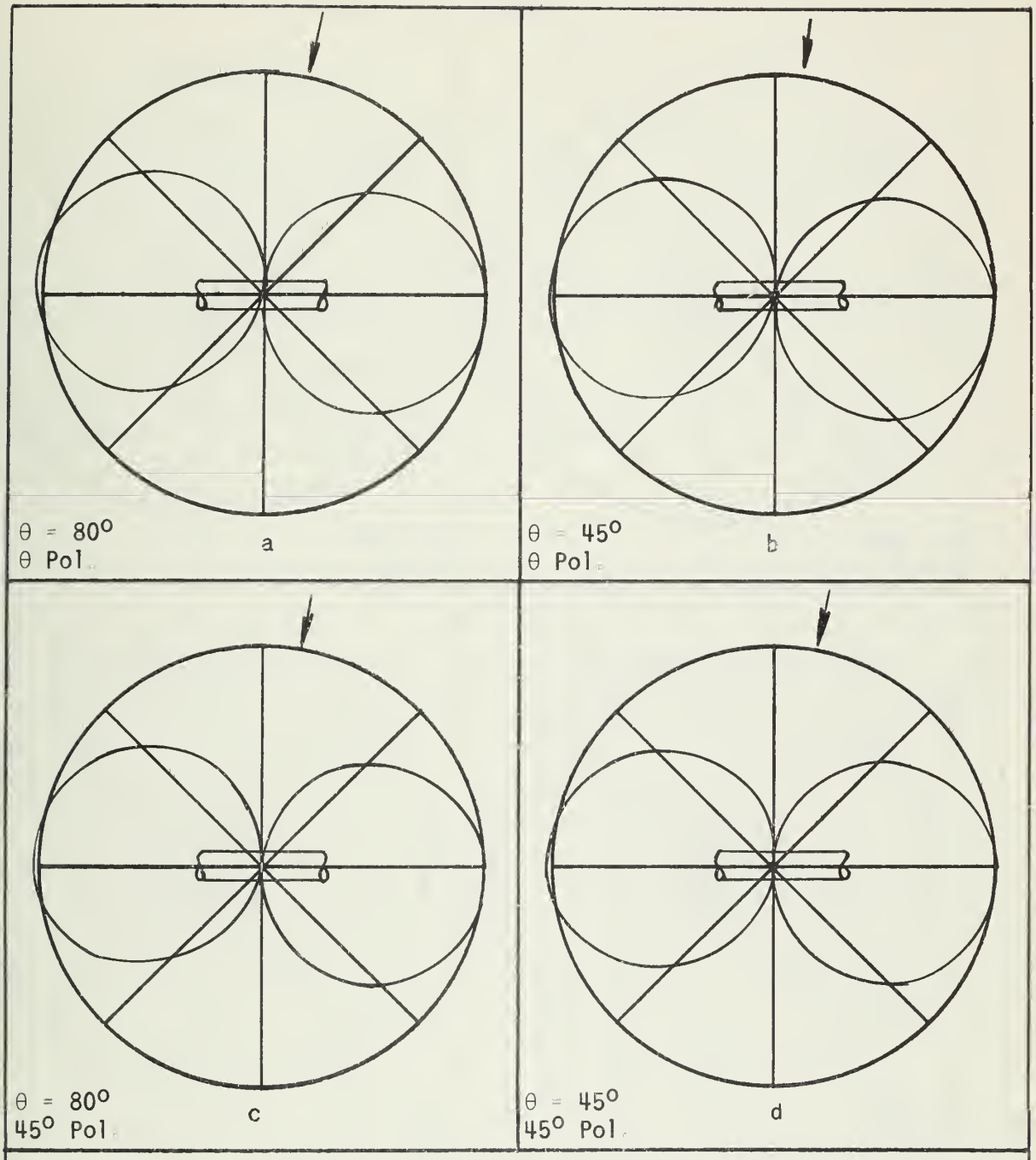

Figure 17 Goniometer Patterns of the Four Loop System Mounted on a Conducting Cylinder of Diameter $\lambda/10$ with the Loop Axes in the Axial Direction of the Cylinder and the Exciting Wave Incident from $\phi = 10^{\circ}$

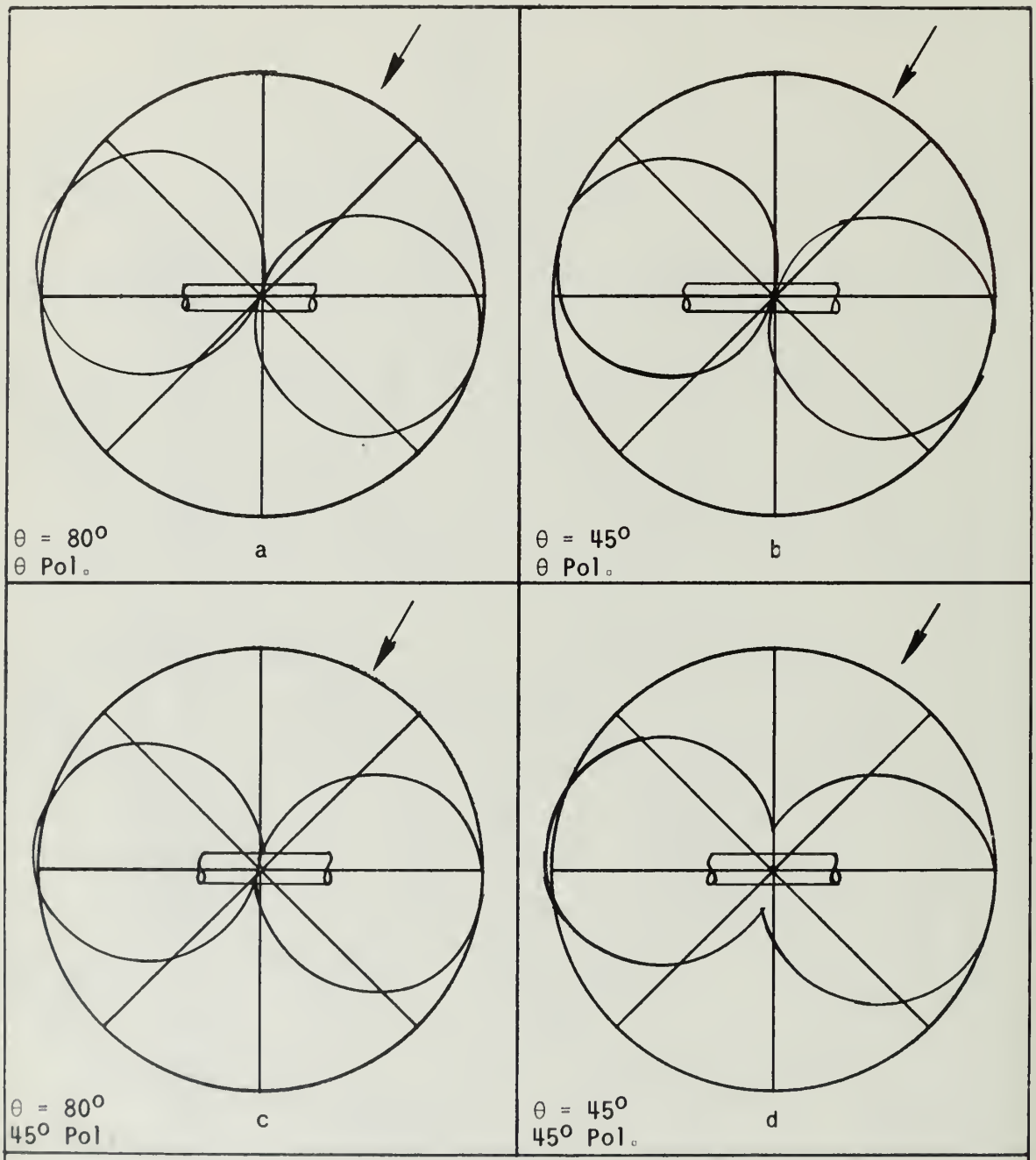

Figure 18 Goniometer Patterns of the Four Loop System Mounted on a Conducting Cylinder of Diameter $\lambda/10$ with the Loop Axes in the Axial Direction of the Cylinder and the Exciting Wave Incident from $\phi = 30^{\circ}$

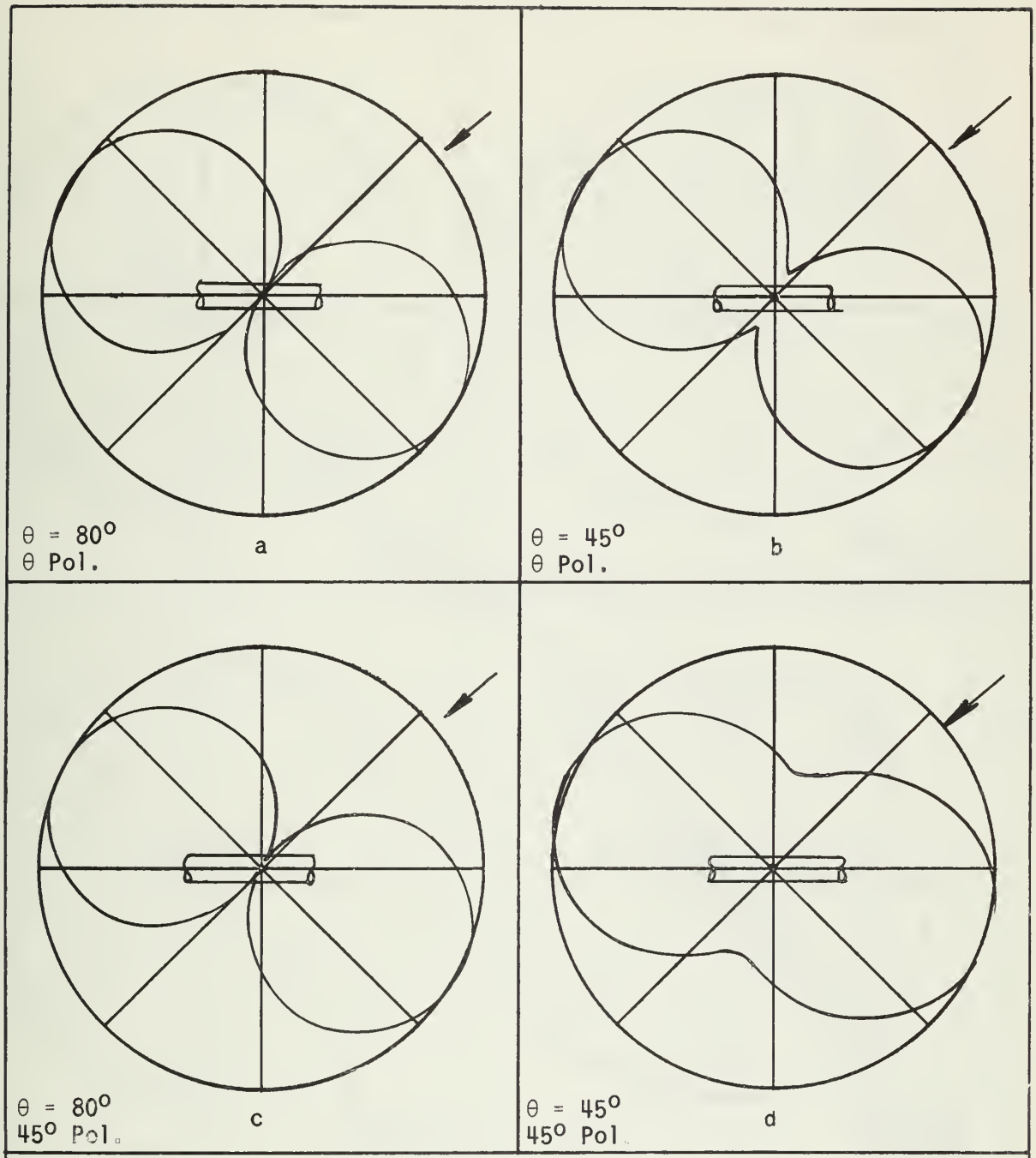

Figure 19 Goniometer Patterns of the Four Loop System Mounted on a Conducting Cylinder of Diameter $\lambda/10$ with the Loop Axes in the Axial Direction of the Cylinder and the Exciting Wave Incident from $\phi = 50^{\circ}$

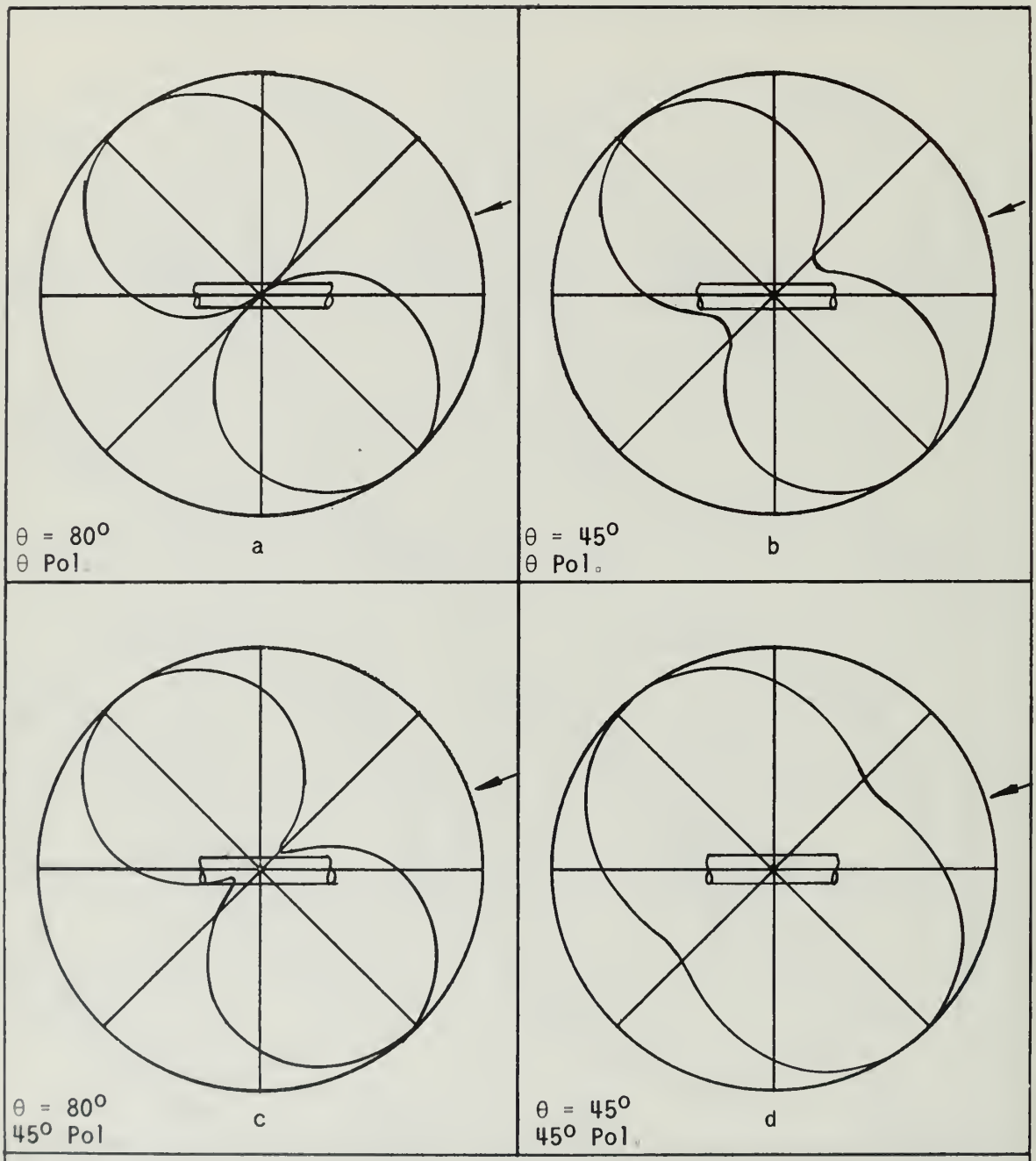

Figure 20 Goniometer Patterns of the Four Loop System Mounted on a Conducting Cylinder of Diameter λ/10 with the Loop Axes in the Axial Direction of the Cylinder and the Exciting Wave Incident from $\phi = 70^{\circ}$

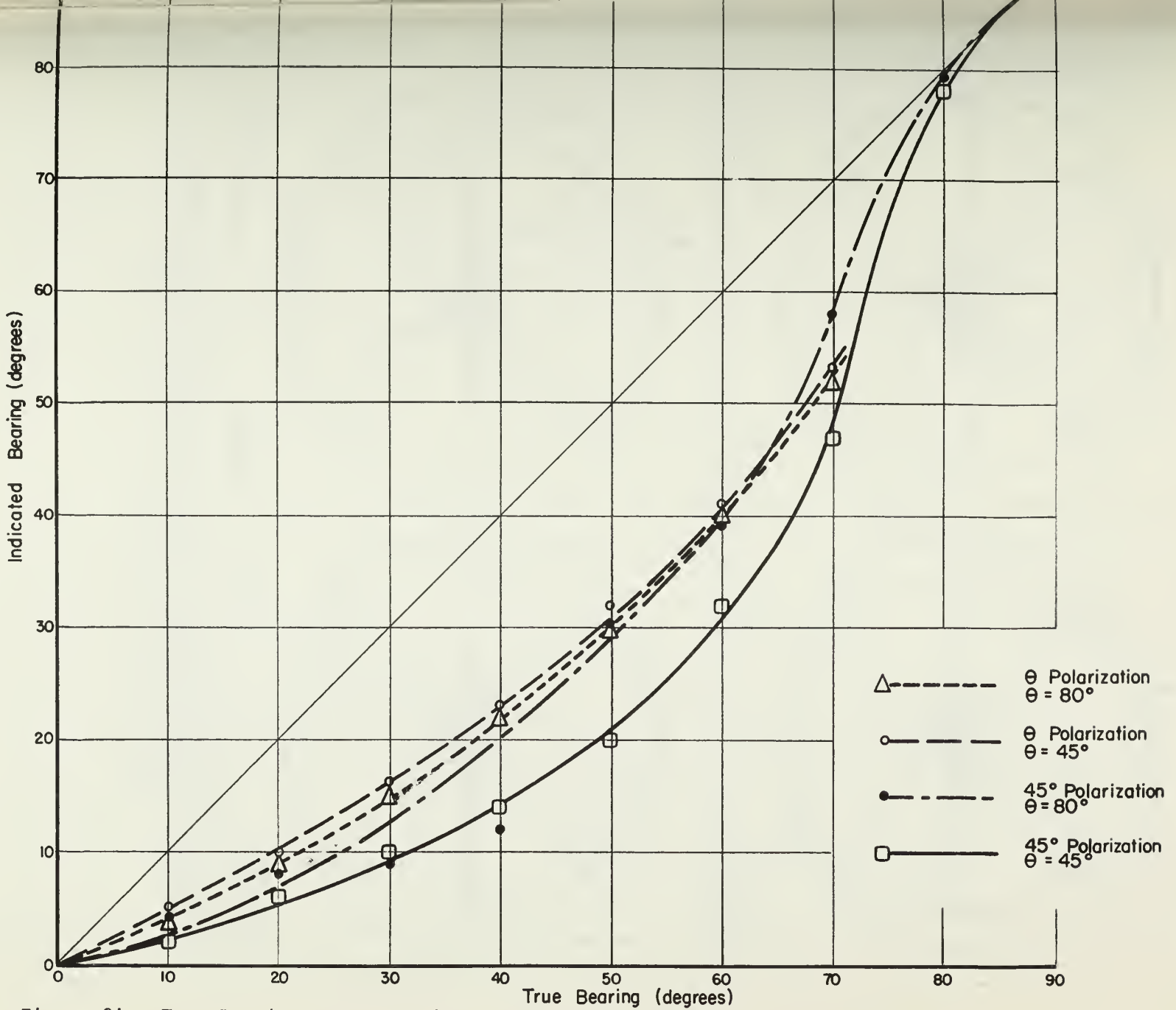

Figure 21. True Bearing versus Indicated Bearing for the Four Loop System Mounted on a Long Cylinder (Axes Axial)

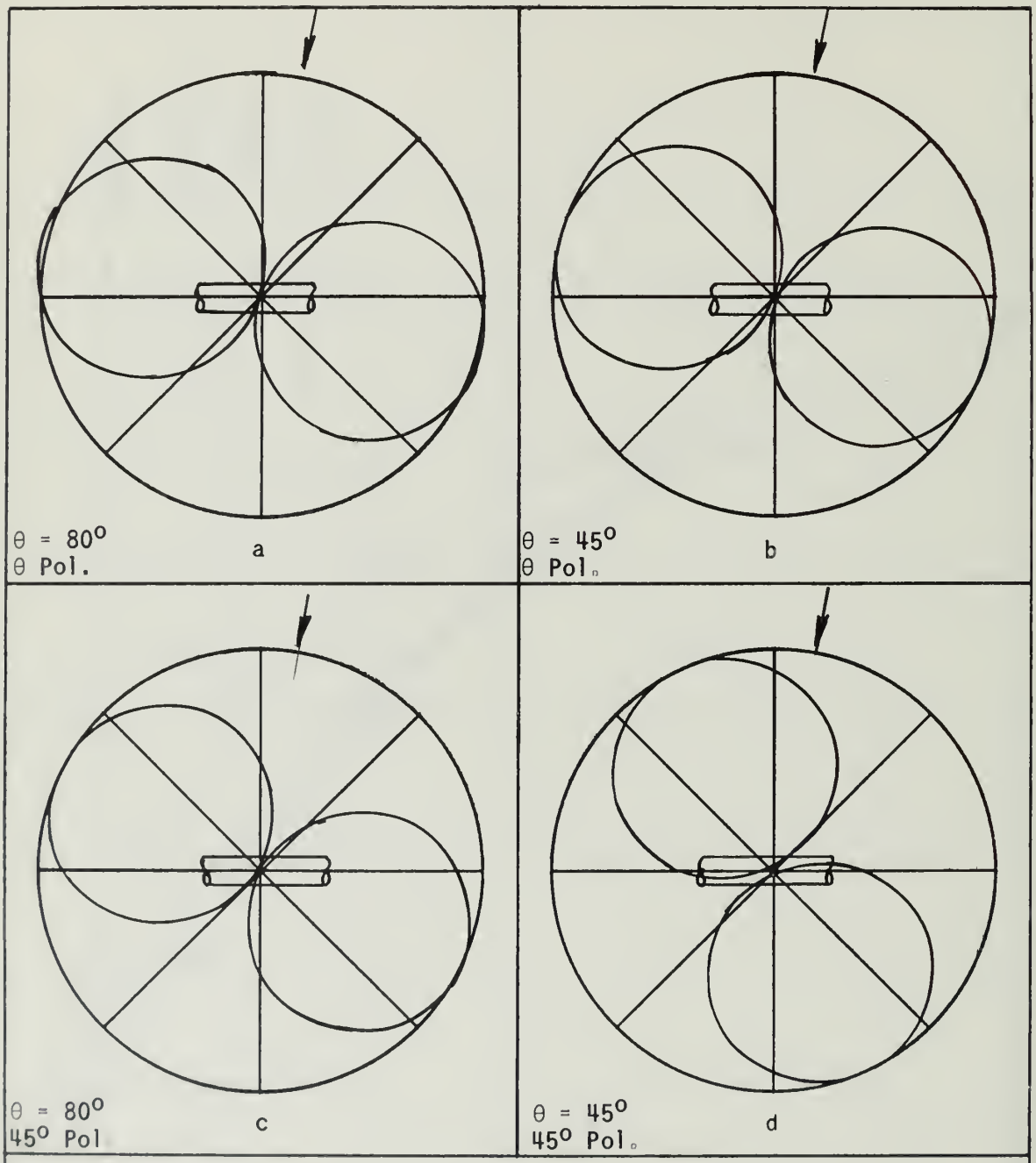

Figure 22 Goniometer Patterns of the Loop System Mounted Above and Below a Conducting Cylinder of Diameter of $\lambda/10$ and Exciting Wave Incident from $\phi = 10^{\circ}$

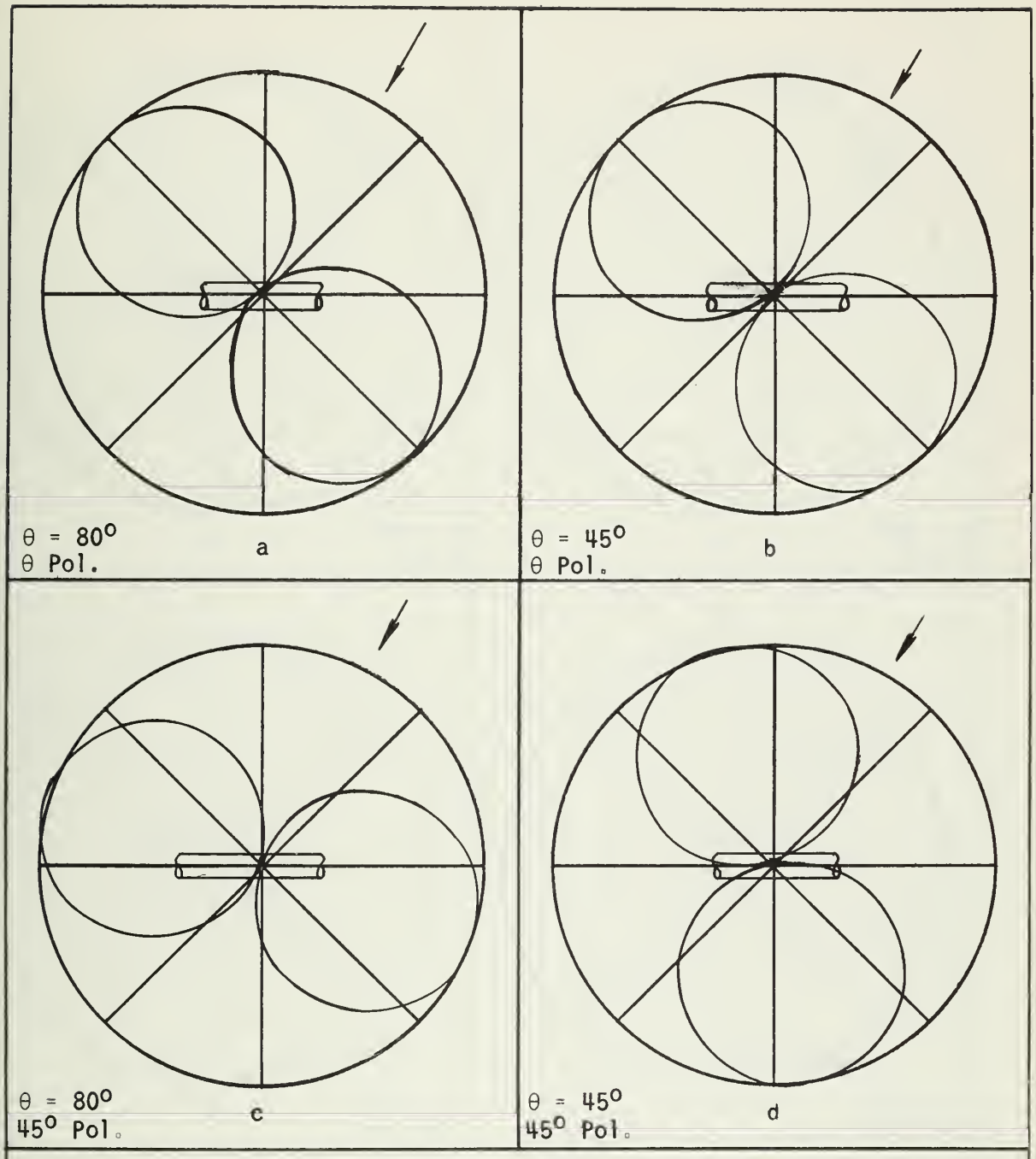

Figure 23. Goniometer Patterns of the Loop System Mounted Above and Below a Conducting Cylinder of Diameter of $\lambda/10$ and Exciting Wave Incident from $\phi = 30^{\circ}$

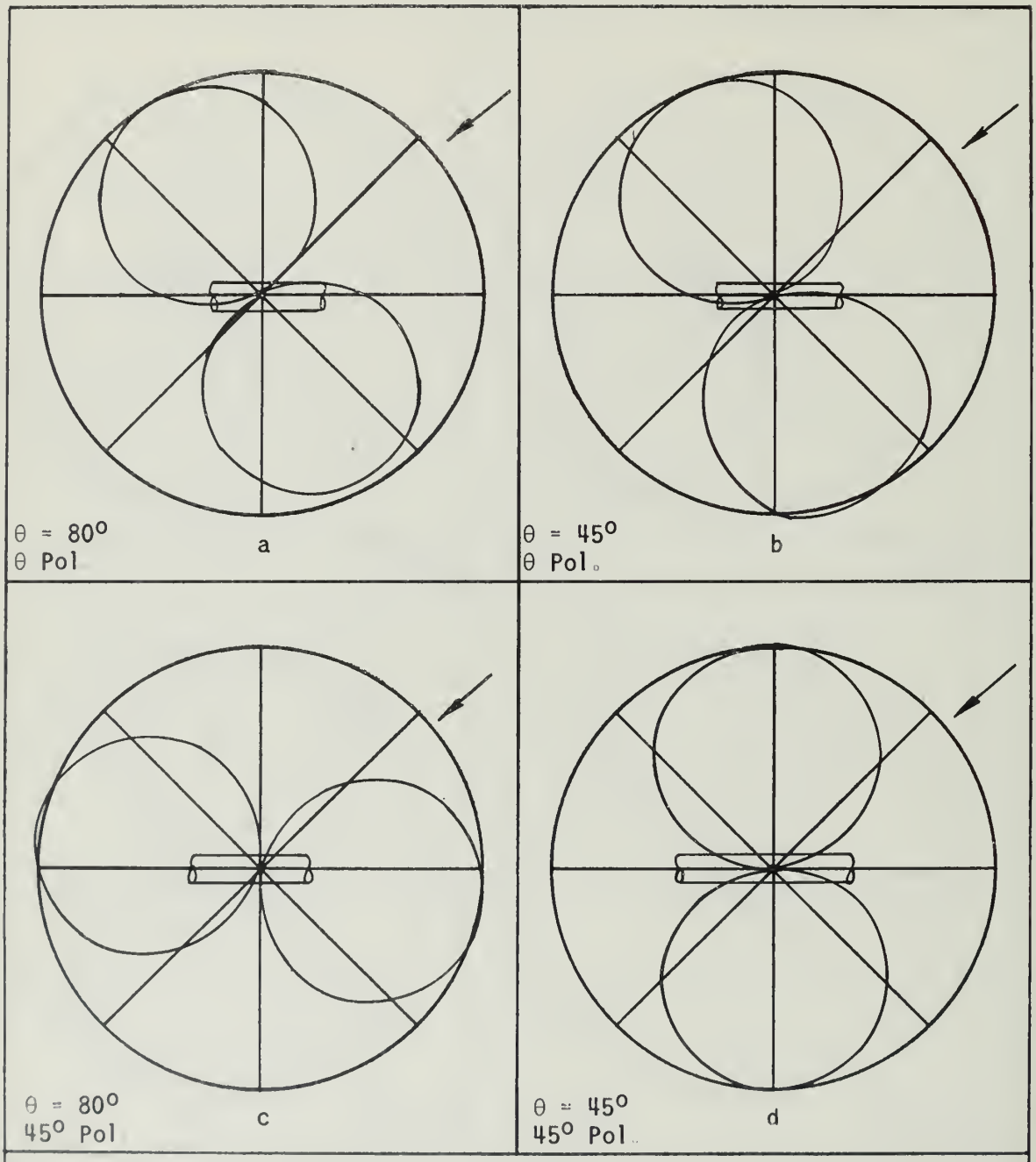

Figure 24. Goniometer Patterns of the Loop System Mounted Above and Below a Conducting Cylinder of Diameter of λ/10 and Exciting Wave Incident from $\phi = 50^{\circ}$

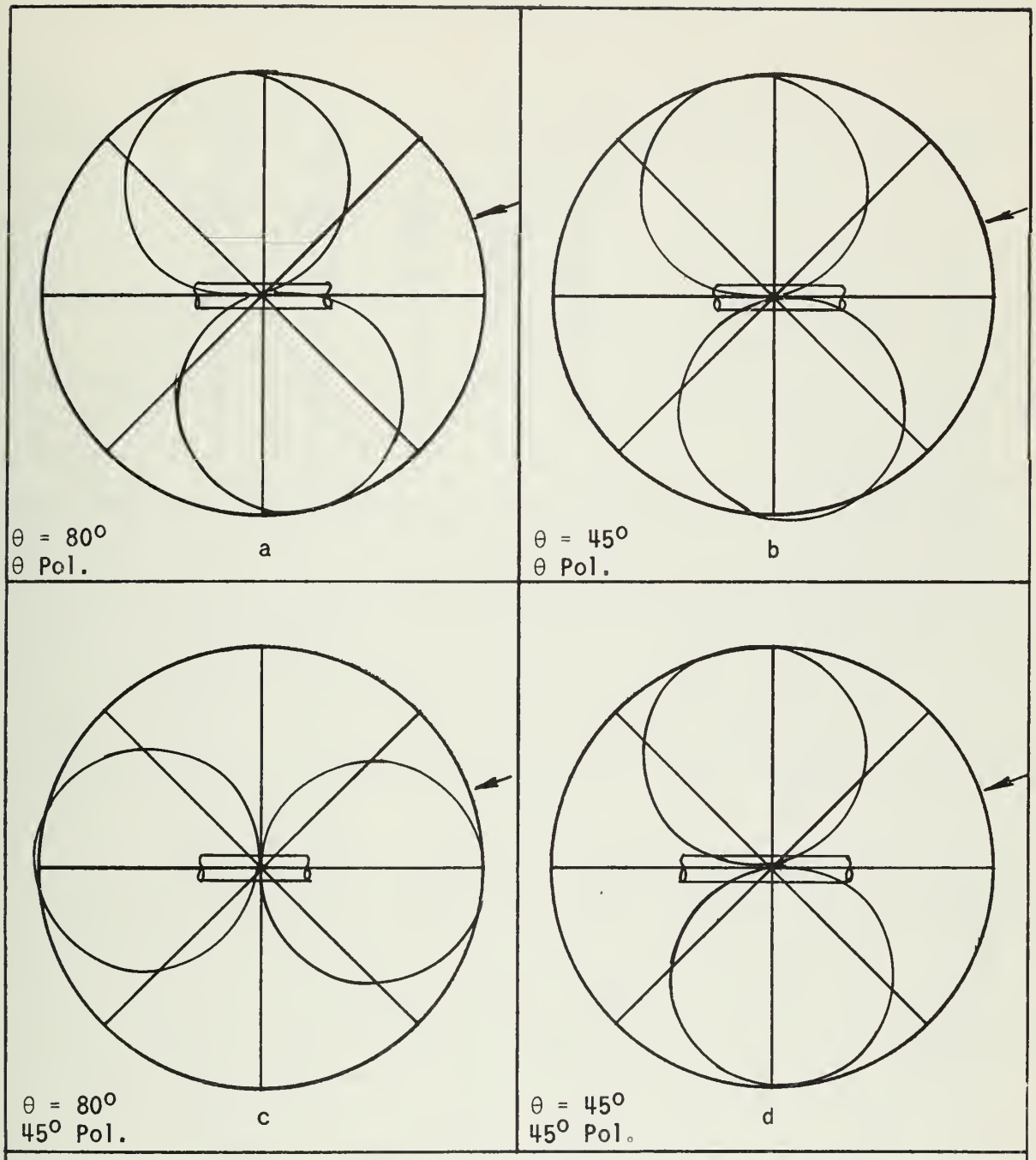

Figure 25. Goniometer Patterns of the Loop System Mounted Above and Below a Conducting Cylinder of Diameter of $\lambda/10$ and Exciting Wave Incident from $\phi = 70^{\circ}$

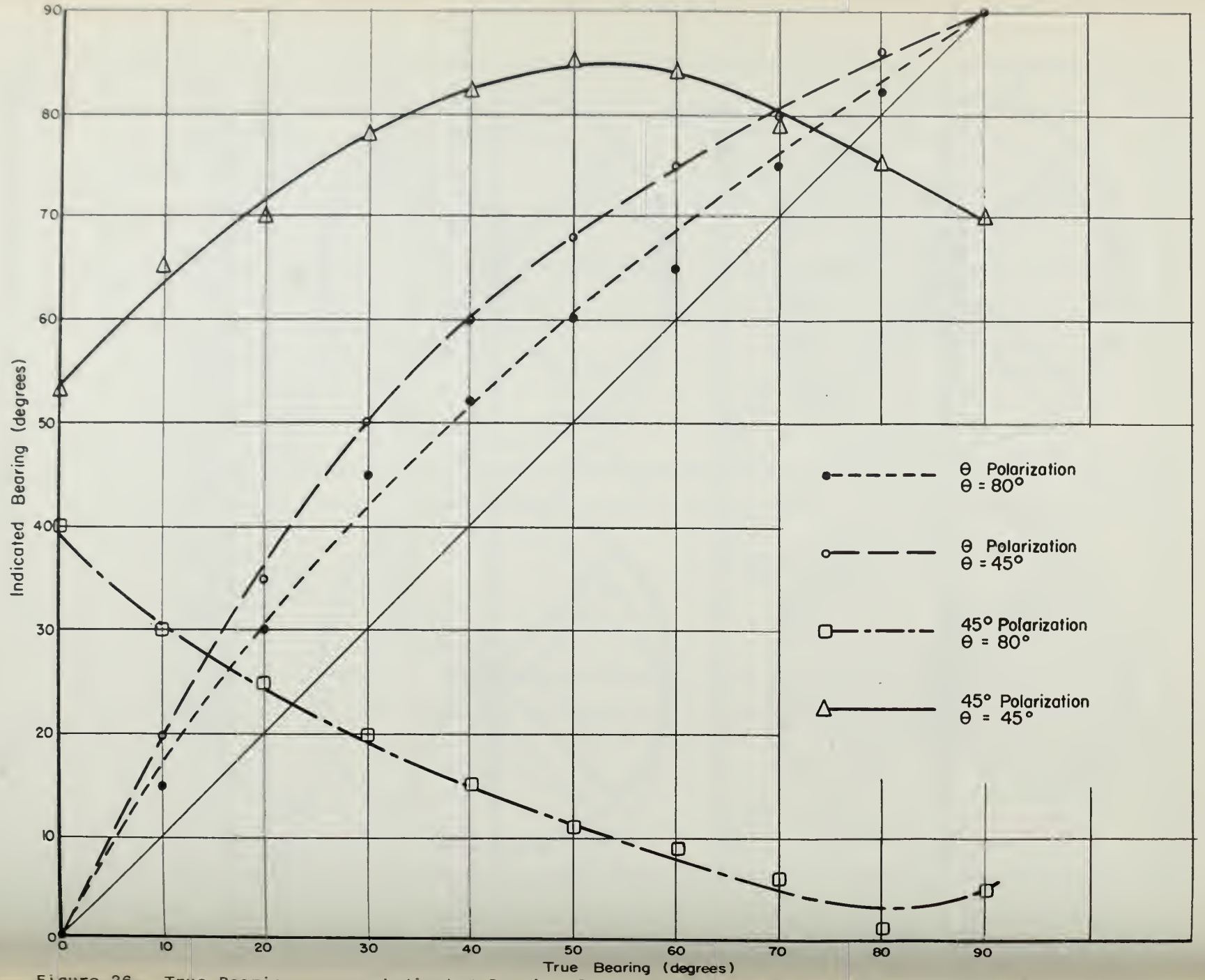

Figure 26. True Bearing versus Indicated Bearing for Crossed Loops Mounted Above and Below the Cylinder

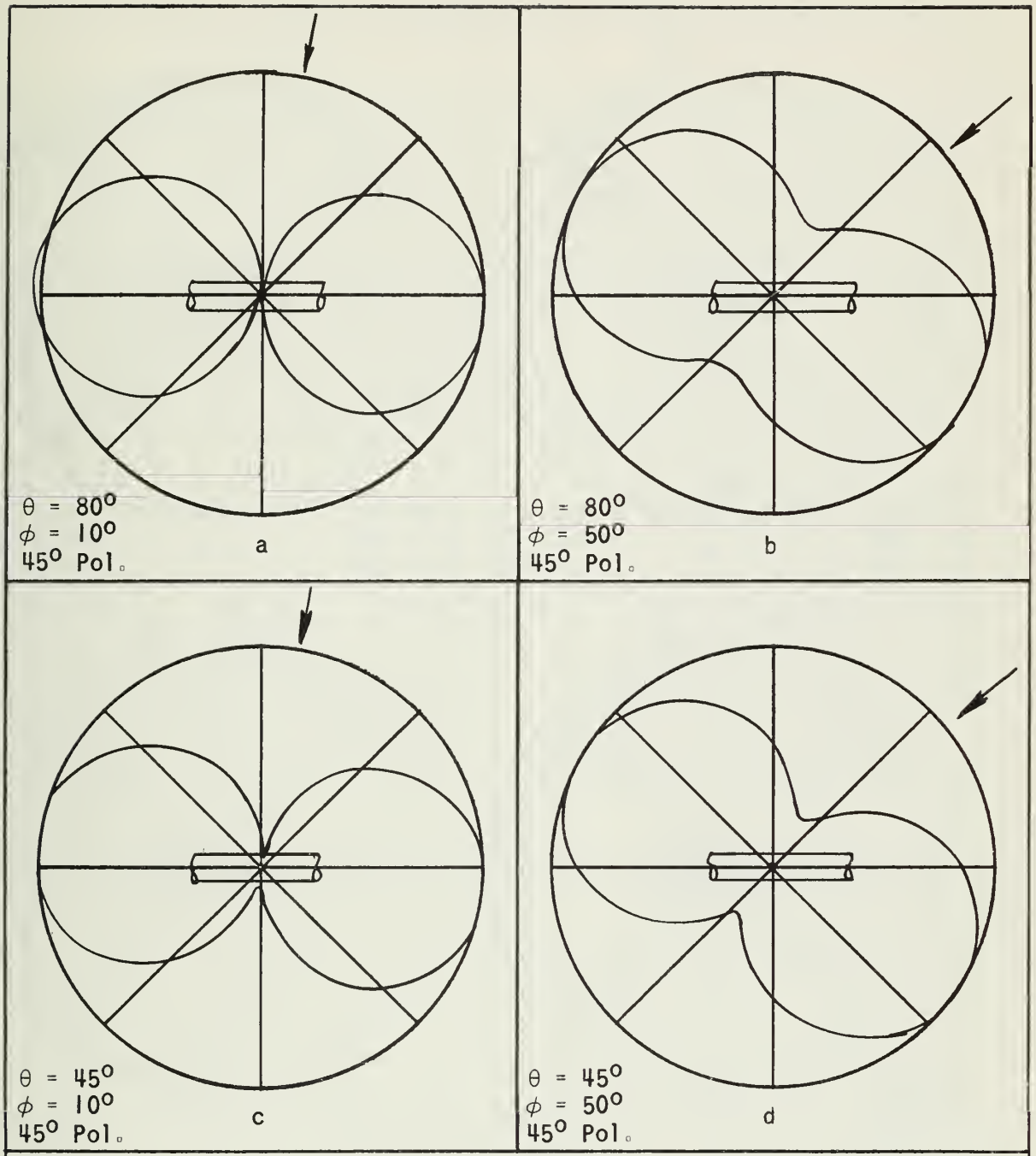

Figure 27. Goniometer Patterns of the Four Loop System Mounted on a Conducting Cylinder of Diameter $\lambda/5$ with the Loop Axes in the Circumferential Direction of the Cylinder.

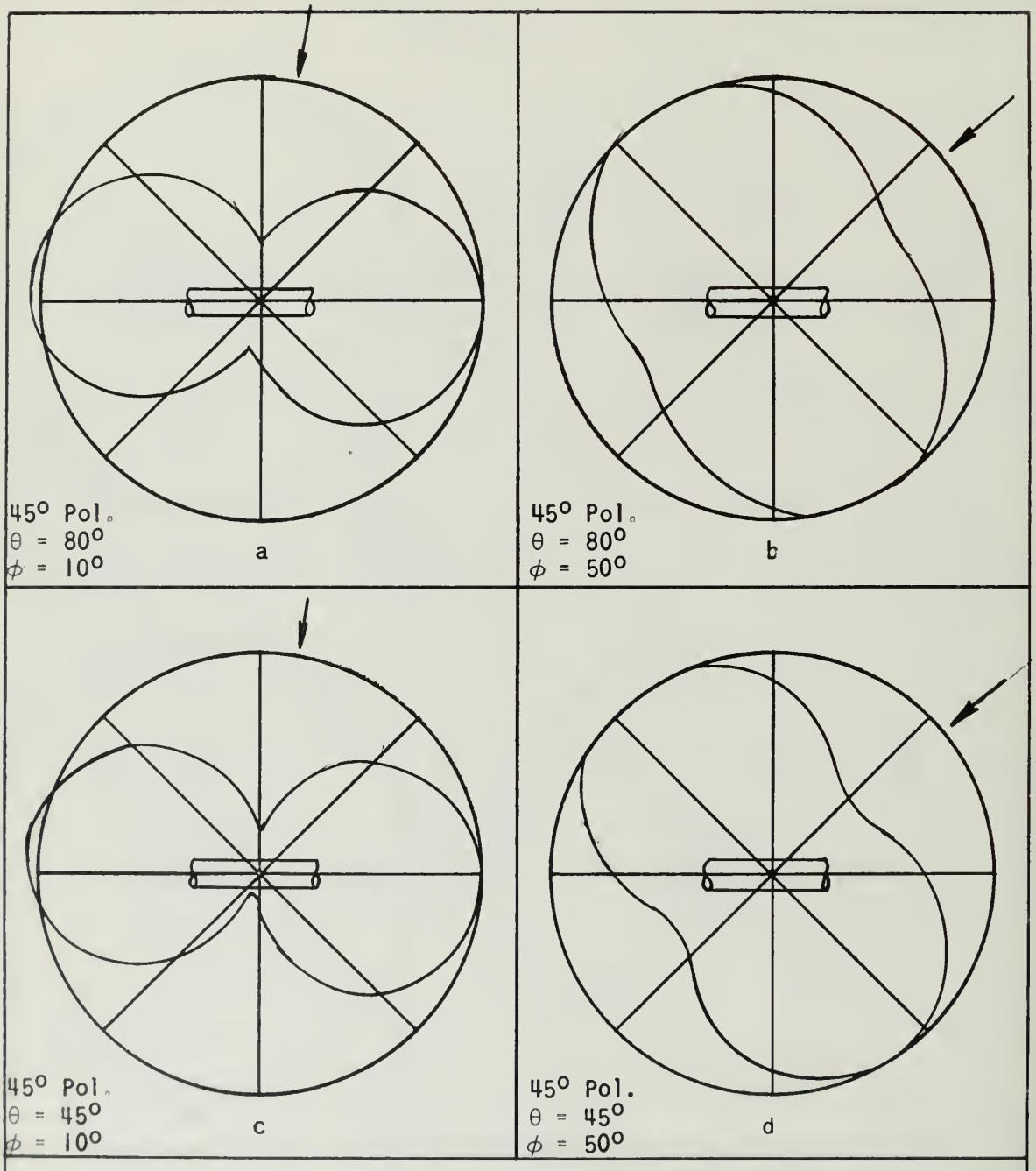

Figure 28 Goniometer Patterns of the Four Loop System Mounted on a Conducting Cylinder of Diameter $\lambda/5$ with the Loop Axes in the Axial Direction of the Cylinder

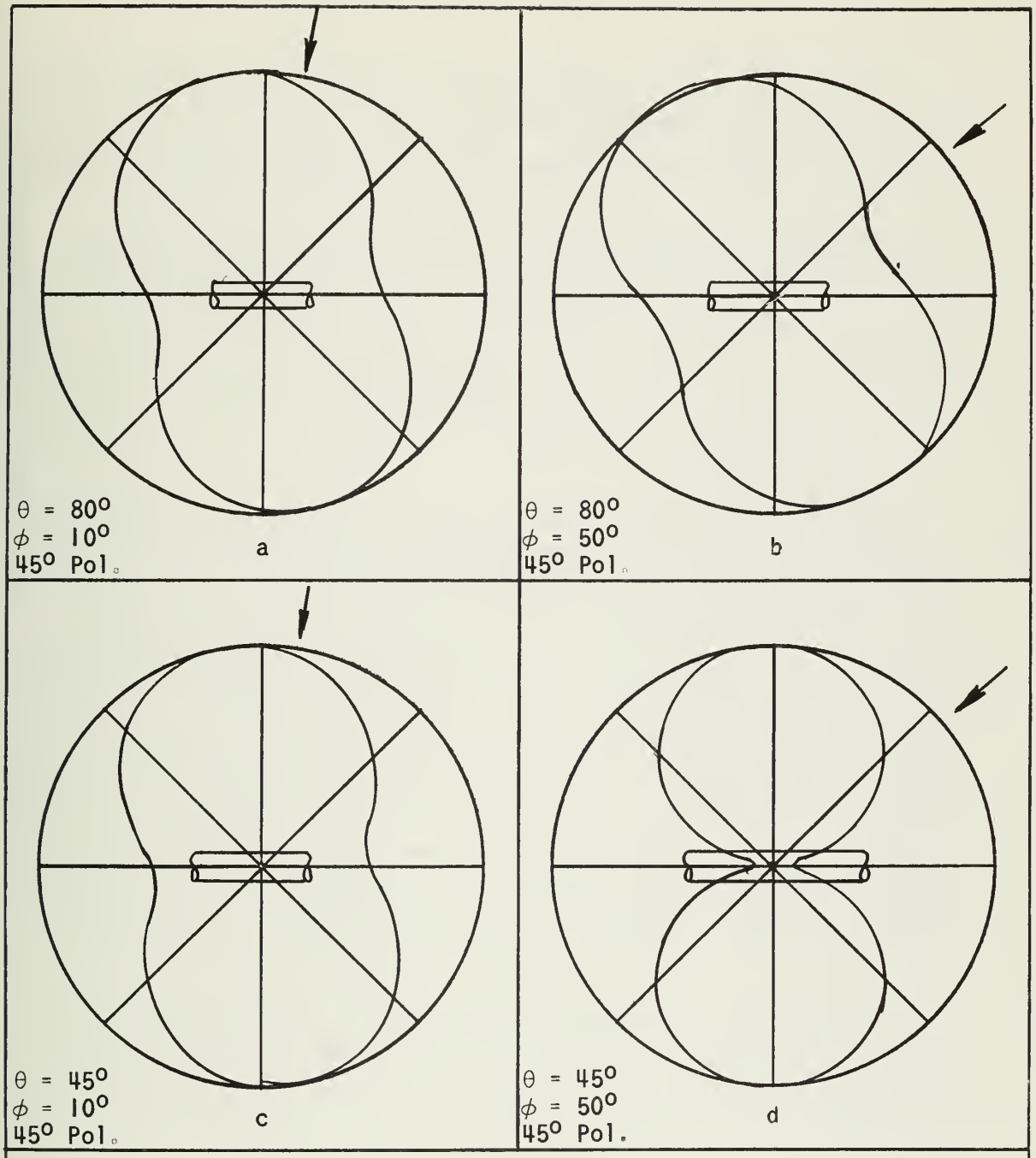

Figure 29. Goniometer Patterns of the Loop System Mounted Above and Below a Conducting Cylinder of Diameter $\lambda/5$

5. CONCLUSIONS

The only encouraging results are those for the spaced loop system with the loop axes oriented in the axial direction of the cylinder. Although the indicated bearings are in considerable error(see Fig. 21), it is seen that the variation of the bearing with polarization is only on the order of ten degrees. This comparatively small polarization error is probably due to the fact that the loops are not coupled to the axial current flowing on the cylinder. Thus, with calibration, this spaced loop system might prove to be fairly accurate when placed on a long narrow body. Since the loop patterns have a null in the axial direction, the system is best suited for signals arriving from directions within about 60^{o} of broadside.

For the spaced loop system with the loop axes circumferential, the large variation of the indicated bearing with polarization (see Fig. 16) makes the system useless for direction finding. For this case, the loops are strongly coupled to the axial current on the cylinder. It is seen that even for θ polarization, the bearing error due to reradiation is quite large. The large variation of the indicated bearing with polarization is also due to the reradiation. It is possible that by using four loops above and four loops below the cylinder (in an attempt to decouple the antenna system from the axial current on the cylinder) that the bearing errors could be reduced. However, the improvement would have to be considerable in order to warrant the added complexity of the antenna system. Unfortunately, time was not available to investigate the eight loop system.

Although this investigation was concerned with loops mounted on conducting cylinders, the results (particularly negative results) can be extended to long, narrow bodies of any shape with circumferences on the order of a wavelength, such as an aircraft wing or fuselage.

BIBLIOGRAPHY

1. "High-Frequency Airborne Direction Finding," *Technical Report No. 30,* Project No. 591, Stanford Research Institute, December 1952.

2. Carter, P. S. "Antenna Arrays Around Cylinders," *Proc. I.R.E.. Vol. 31,* 671-693, December 1943.

3. Sinclair, G. "The Patterns of Antennas Located Near Cylinders of Elliptical Cross Section," *Proc., I.R.E., Vol. 39,* 660-668, June 1951.

APPENDIX I

A plane wave from the direction described by ϕ and θ with the magnetic field in the θ direction (Fig. 30) has rectangular components

$$H_z = -H_\theta \sin \theta \tag{1}$$

$$H_y = H_\theta \cos \theta \sin \phi \tag{2}$$

$$H_x = H_\theta \cos \theta \cos \phi \tag{3}$$

where $H_\theta = H_{\theta_o} e^{j\beta r}$. (4)

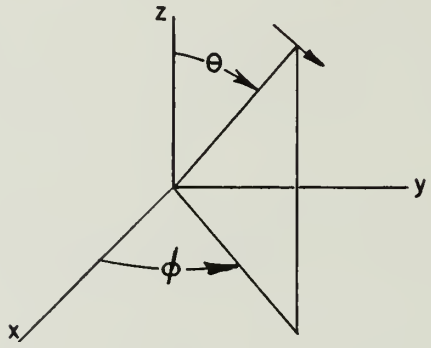

Figure 30. Spherical Coordinate System

The voltage induced by this wave in four loops with axes in the x direction, located at x = 0, y = ±d/2, and y = 0, x = ±d/2, (Fig. 31) are, for the loop at y = +d/2,

$$V_{\theta_1} = H_x (0, d/2, 0)$$
$$= H_{\theta_o} \cos \theta \cos \phi \, e^{j\beta(r_o - d/2 \sin \phi)}. \tag{5}$$

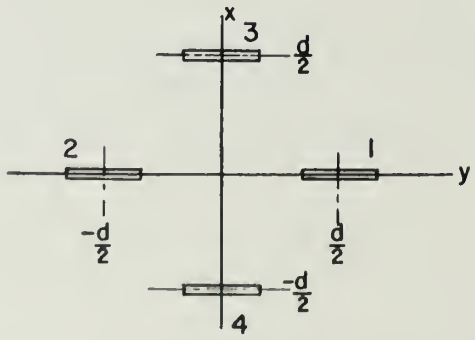

Figure 31 Location of the Four Loops

for the loop located at y = -d/2

$$V_{\theta_2} = H_x(0, -d/2, 0)$$
$$= H_{\theta_0} \cos\theta \cos\phi \, e^{j\beta(r_0 + d/2 \sin\phi)} \quad (6)$$

for the loop located at x = +d/2

$$V_{\theta_3} = H_x(d/2, 0, 0)$$
$$= H_{\theta_0} \cos\theta \cos\phi \, e^{j\beta(r_0 - d/2 \cos\phi)} \quad (7)$$

and for the loop located at x = -d/2

$$V_{\theta_4} = H_x(-d/2, 0, 0)$$
$$= H_{\theta_0} \cos\theta \cos\phi \, e^{j\beta(r_0 + d/2 \cos\phi)}. \quad (8)$$

To get the voltage of loops one and two when connected out of phase, Eq. 6 is subtracted from Eq. 5.

$$V_{\theta_{1-2}} = H_{\theta_0} \cos\theta \cos\phi \left[e^{j\beta(r_0 - d/2 \sin\phi)} - e^{j\beta(r_0 + d/2 \sin\phi)} \right]$$
$$= -2jH_{\theta_0} \cos\theta \cos\phi \, e^{j\beta r_0} \sin(\beta d/2 \sin\phi). \quad (9)$$

The voltage of loops three and four connected out of phase is determined by subtracting Eq. 8 from Eq. 7.

$$V_{\theta_{3-4}} = H_{\theta_0} \cos\theta \cos\phi \, e^{j\beta(r_0 - d/2 \cos\phi)} - e^{j\beta(r_0 + d/2 \cos\phi)}$$
$$= -2jH_{\theta_0} \cos\theta \cos\phi \, e^{j\beta r_0} \sin(\beta d/2 \cos\phi). \quad (10)$$

For a plane wave with H in the ϕ direction the rectangular components are

$$H_z = 0 \quad (11)$$
$$H_y = H_\phi \cos\phi \quad (12)$$
$$H_x = H_\phi \sin\phi \quad (13)$$

where $H_\phi = H_{\phi_0} \, e^{j\beta r}$. (14)

In a manner similar to the foregoing, the output voltages of loops one and two connected out of phase and of loops three and four connected out

of phase that are induced by this ϕ-polarized wave are

$$V_{\phi_{1-2}} = -2jH_{\phi_o} \sin \phi \, e^{j\beta r_o} \sin (\beta \, d/2 \sin \phi) \tag{15}$$

$$V_{\phi_{3-4}} = -2jH_{\phi_o} \sin \phi \, e^{j\beta r_o} \sin (\beta \, d/2 \cos \phi) \, . \tag{16}$$

If α is the angle of polarization (Fig. 32) then

$$H_{\theta_o} = H_o \cos \alpha \tag{17}$$

$$H_{\phi_o} = H_o \sin \alpha \tag{18}$$

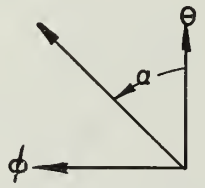

Figure 32. Definition of Polarization Angle, α

Substituting Eqs. 17 and 18 into Eqs. 9,, 10, 15, and 16 yields

$$V_{\theta_{1-2}} = -2jH_o \cos \alpha \cos \theta \cos \phi \, e^{j\beta r_o} \sin (\beta \, d/2 \sin \phi) \tag{19}$$

$$V_{\theta_{3-4}} = -2jH_o \cos \alpha \cos \theta \cos \phi \, e^{j\beta r_o} \sin (\beta \, d/2 \cos \phi) \tag{20}$$

$$V_{\phi_{1-2}} = -2jH_o \sin \alpha \sin \phi \, e^{j\beta r_o} \sin (\beta \, d/2 \sin \phi) \tag{21}$$

$$V_{\phi_{3-4}} = -2jH_o \sin \alpha \sin \phi \, e^{j\beta r_o} \sin (\beta \, d/2 \cos \phi) \, . \tag{22}$$

In order to get the total voltage induced in the loop pairs by a wave of α polarization, Eqs. 19 and 21 are added as are Eqs. 20 and 22.

$$V_{\text{total}_{1-2}} = -2jH_o \, e^{j\beta r_o} \sin (\beta \, d/2 \sin \phi)(\cos \alpha \cos \theta \cos \phi + \sin \alpha \sin \phi)$$

$$= K \sin(\beta \, d/2 \sin \phi) \, (\cos \alpha \cos \theta \cos \phi + \sin \alpha \sin \phi) \tag{23}$$

$$V_{\text{total}_{3-4}} = -2jH_o \, e^{j\beta r_o} \sin(\beta \, d/2 \cos \phi) \, (\cos \alpha \cos \theta \cos \phi + \sin \alpha \sin \phi)$$

$$= K \sin(\beta \, d/2 \cos \phi) \, (\cos \alpha \cos \theta \cos \phi + \sin \alpha \sin \phi). \tag{24}$$

If a goniometer is used that multiplies Eq. 23 by cos γ and Eq. 24 by sin γ (where γ is the goniometer angle) and then subtracts the two, the result is

$$V_{\text{goniometer}} = K[\sin(\beta \, d/2 \sin \phi) \cos \gamma - \sin(\beta \, d/2 \cos \phi) \sin \gamma]$$

$$X[\cos \alpha \cos \theta \cos \phi + \sin \alpha \sin \phi] \tag{25}$$

which for small β d/2 (closely spaced loops) becomes

$$V_{goniometer} \cong K (\sin \phi \cos \gamma - \cos \phi \sin \gamma)$$

$$= X (\cos \alpha \cos \theta \cos \phi + \sin \alpha \sin \phi)$$

$$= K \sin (\phi - \gamma) (\cos \alpha \cos \theta \cos \phi + \sin \alpha \sin \phi) \qquad (26)$$

which has a null at $\gamma = \phi$, regardless of θ, ϕ, or α.

APPENDIX II

The equations of Carter[1] and Sinclair[2] for the patterns of a small antenna near a long conducting cylinder were derived for a cylinder vertically oriented, i.e., lying along the z-axis of the ordinary right hand coordinate system. For the purposes of the work reported here (where the cylinder was to represent a horizontal wing or fuselage), it was desirable to have the cylinder oriented in a horizontal position. Consequently a transformation of coordinates was necessary. The primed coordinates (θ', ϕ') are used in the equations for the vertical cylinder while the standard θ and ϕ coordinates indicate the direction of arrival of the plane wave. Figure 33 illustrates the coordinate systems with respect to the cylinder.

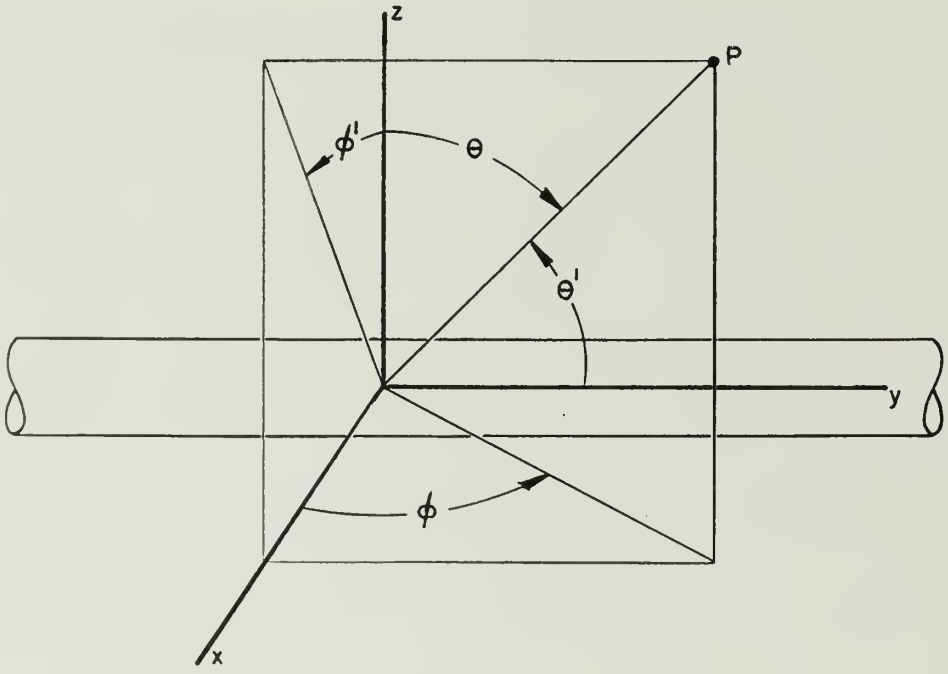

Figure 33 Definition of the Coordinates

As an example, let us say that the antenna's response to a signal arriving from a certain direction, $\theta = \theta_1$, and $\phi = \phi_1$, is desired. The equations that will determine this response are in terms of the primed coordinates. Hence it is necessary to transform the given θ, and ϕ into the corresponding values of θ', and ϕ'. It can be shown, using

spherical trigonometry, that the equations of transformation are

$$\phi_1' = \tan^{-1}(\tan \theta_1 \cos \phi_1) \tag{27}$$

$$\theta_1' = \cos^{-1}(\sin \theta_1 \sin \phi_1) \ . \tag{28}$$

Applying these values of ϕ_1' and θ_1' to the equations yields the desired response in terms of the voltages induced in the antenna by the ϕ' and θ' components of incident field. The voltages induced in the antenna can then be obtained in terms of the θ and ϕ components of incident field by the use of the following equations;

$$V_\theta = V_{\phi'} \sin \alpha - V_{\theta'} \cos \alpha \tag{29}$$

$$V_\phi = -V_{\phi'} \cos \alpha - V_{\theta'} \sin \alpha \tag{30}$$

where

$$\alpha = \cos^{-1} \frac{\sin \phi \cos \theta}{\sin \theta'} \ . \tag{31}$$

The equations for $V_{\phi'}$ and $V_{\theta'}$ of a small loop near a long conducting cylinder as taken from Sinclair[2] are:

For a loop the axis of which is in the axial direction of the cylinder

$$V_{\phi'} = \frac{-ej\beta z \sin \theta'}{\eta} \sum_{n=0}^{\infty} \varepsilon_n (j)^n [J_n(w) + C_n' H_n^{(2)}(w)] \cos n(\phi' - \phi_o') \tag{32}$$

$$V_{\theta'} = 0. \tag{33}$$

For a loop the axis of which is in the circumferential direction of the cylinder

$$V_{\theta'} = \frac{je^{j\beta z \cos \theta'}}{\eta} \sum_{n=0}^{\infty} \varepsilon_n (j)^n [J_n'(w) + C_n H_n'^{(2)}(w)] \cos n(\phi' - \phi_o') \tag{34}$$

$$V_{\phi'} = \frac{-j \cos \theta' e^{j\beta z \cos \theta'}}{\eta w} \sum_{n=0}^{\infty} \varepsilon_n (j)^n n [J_n(w) + C_n' H_n^{(2)}(w)] \sin n(\phi' - \phi_o') \tag{35}$$

where

ϕ_o' is the location of the loop around the cylinder

$w = \beta b \sin \theta'$

$$C_n' = - \frac{J_n'(\beta a \sin \theta')}{H_n'^{(2)}(\beta a \sin \theta')}$$

$$C_n = - \frac{J_n(\beta a \sin \theta')}{H_n^{(2)}(\beta a \sin \theta')}$$

a is the radius of the cylinder

b is the radial distance of the loop from the cylinder axis

ε_n = Neumann's number = $\begin{matrix} 1 \text{ for } n = 0 \\ 2 \text{ for } n \neq 0 \end{matrix}$

J_n, $H_n^{(2)}$, J_n', $H_n'^{(2)}$ are the appropriate solutions of Bessel's equation and their derivatives with respect to w.

The patterns of the multiple loop configuration illustrated in Fig. 3 can be obtained from Eqs. 34 and 35. Allowing b = a = $\lambda/20$ (flush mounted loops), the patterns of loops one and two mounted at z = 0, $\phi' = \pm 14.3^o$ (making the circumferential distance between the two equal to $\lambda/40$) and connected out of phase are described by

$$V_{\theta_{1-2}'} = \frac{-4}{\eta \pi w} \sum_{n=1}^{\infty} \frac{(j)^n [\cos n(\phi' - 14.3^o) - \cos n(\phi' + 14.3)]}{H_n^{(2)}(w)} \tag{36}$$

$$V_{\phi_{1-2}'} = \frac{-4 \cos \theta'}{\eta \pi w^2} \sum_{n=1}^{\infty} \frac{(j)^n [\sin n(\phi' - 14.3^o) - \sin n(\phi' + 14.3^o)]}{-\frac{n}{w} H_n^{(2)}(w) + H_{n-1}^{(2)}(w)}. \tag{37}$$

The patterns of loops three and four mounted at $\phi' = 0$, z = $\pm\lambda/80$ and connected out of phase are described by

$$V_{\theta_{3-4}'} = \frac{-2 \sin \frac{\pi \cos \theta'}{40}}{\eta} \sum_{n=1}^{\infty} \varepsilon_n (j)^n [J_n'(w) + C_n H_n^{(2)'}(w)] \cos n \phi' \tag{38}$$

$$V_{\phi_{3-4}'} = \frac{4 \sin \frac{\pi \cos \theta'}{40}}{\eta \frac{\pi}{10} \sin \theta'} \sum_{n=1}^{\infty} (j)^n n [J_n(w) + C_n' H_n^{(2)}(w)] \sin n \phi'. \tag{39}$$

Figure 4 illustrates the same loop system as Fig. 3 as far as spacing, location, and connection are concerned. The difference is that the loops have now been rotated by 90°. The patterns of the pairs

of loops oriented in this manner can be obtained from Eqs. 32 and 33 and are described by

$$V_{\theta'_{1-2}} = 0$$

$$V_{\phi'_{1-2}} = \frac{-4 \sin \theta'}{\eta} \sum_{n=1}^{\infty} (j)^n [J_n(w) + C'_n H_n^{(2)}(w)] \sin n \phi' \sin n\, 14.3^o \qquad (40)$$

$$V_{\theta'_{3-4}} = 0$$

$$V_{\phi'_{3-4}} = -2j \sin \frac{\pi \cos \theta'}{40} \frac{\sin \theta'}{\eta} \sum_{n=0}^{\infty} \varepsilon_n (j)^n [J_n(w) + C'_n H_n^{(2)}(w)] \cos n \phi'. \qquad (41)$$

The patterns of the loop system illustrated in Fig. 5 can be obtained from Eqs. 32, 33, 34, and 35. The loops are flush mounted at $z = 0$, $\phi' = 0$ and π. The equations describing these patterns are

$$V_{\theta'_{1-2}} = \frac{2j}{\eta} \sum_{n \text{ odd}} \varepsilon_n (j)^n [J'_n(w) + C_n H_n'^{(2)}(w)] \cos n \phi' \qquad (42)$$

$$V_{\phi'_{1-2}} = \frac{-4j \cos \theta'}{\eta \frac{\pi}{10} \sin \theta'} \sum_{n \text{ odd}} \varepsilon_n (j)^n [J_n(w) + C'_n H_n^{(2)}(w)] \sin n \phi' \qquad (43)$$

$$V_{\theta'_{3-4}} = 0 \qquad (44)$$

$$V_{\phi'_{3-4}} = \frac{-2 \sin \theta'}{\eta} \sum_{n \text{ even}} \varepsilon_n (j)^n [J_n(w) + C'_n H_n^{(2)}(w)] \cos n \phi'. \qquad (45)$$

If S_1 and S_2 are two signals that are fed into a sine, cosine multiplying goniometer, the square of the magnitude of the goniometer output voltage will be

$$|V_{\text{goniometer}}|^2 = |S_1|^2 \sin^2 \gamma + |S_2|^2 \cos^2 \gamma - 2|S_1||S_2| \sin \gamma \cos \gamma \cos \beta \qquad (46)$$

where γ is the goniometer angle of rotation and β is the angle between the complex values of S_1 and $-S_2$ (see Fig. 34). For the systems illustrated in Figs. 3 and 4, V_{1-2} was chosen as S_1 and V_{3-4} as S_2. For the system of Fig. 5, V_{3-4} was used as S_1 and V_{1-2} as S_2.

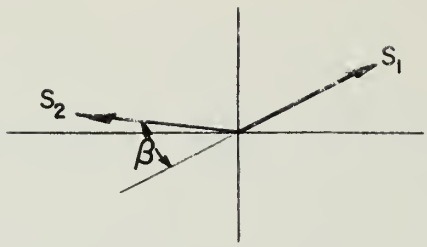

Figure 34. Definition of β

DISTRIBUTION LIST FOR TECHNICAL REPORTS ISSUED UNDER CONTRACT AF33(616)-3220

One copy each unless otherwise indicated

Contractor
Wright Air Development Center
Wright-Patterson Air Force Base, Ohio

Attn: Mr. E. M. Turner, WCLRS-6
4 copies

Commander
Wright Air Development Center
Wright-Patterson Air Force Base, Ohio

Attn: Mr. N. Draganjac, WCLNT-4

Armed Services Technical Information Agency
Knott Building
4th and Main Streets 5 copies
Dayton 2, Ohio 1 repro.

Attn: DSC-SA (Reference AFR205-43)

Commander
Hq. A. F. Cambridge Research Center
Air Research and Development Command
Laurence G. Hanscom Field
Bedford, Massachusetts

Commander
Hq. A.F. Cambridge Research Center
Air Research and Development Command
Laurence G. Hanscom Field
Bedford, Massachusetts

Attn: CRTOTL-1

Commander
Hq. A.F. Cambridge Research Center
Air Research and Development Command
Laurence G. Hanscom Field
Bedford, Massachusetts

Attn: CRRD, R. E. Hiatt

Air Force Development Field
Representative
Attn: Major M. N. Abramovich
Code 1110
Naval Research Laboratory
Washington 25, D. C.

Director
Ballistics Research Lab.
Aberdeen Proving Ground, Maryland

Attn: Ballistics Measurement Lab.

Office of the Chief Signal Officer
Attn: SIGNET-5
Eng. & Technical Division
Washington 25, D. C.

Commander
Rome Air Development Center
Attn: RCERA-1 D. Mather
Griffiss Air Force Base
Rome, New York

Director
Evans Signal Laboratory
Belmar, New Jersey

Attn: Mr. O. C. Woodyard

Director
Evans Signal Laboratory
Belmar, New Jersey

Attn: Mr. S. Krevsky

Director
Evans Signal Laboratory
Belmar, New Jersey

Attn: Technical Document Center

Naval Air Missile Test Center
Point Mugu, California

Attn: Antenna Section

Commander
U. S. Naval Air Test Center
Attn: ET-315
Antenna Section
Patuxent River, Maryland

Beech Aircraft Corporation
Attn: Chief Engineer
6600 E. Central Avenue
Wichita 1, Kansas
M/F Contract AF33(600)-20910

Bell Aircraft Corporation
Attn: Mr. J. D. Shantz
Buffalo 5, New York
M/F Contract W-33(038)-14169

Boeing Airplane Company
Attn: G. L. Hollingsworth
7755 Marginal Way
Seattle, Washington
M/F Contract AF33(038)-21096

Grumman Aircraft Engineering Corp.
Attn: J. S. Erickson,
Chief Engineer
Bethpage
Long Island, New York
M/F Contract NOa(s) 51-118

Hallicrafters Corporation
Attn: Norman Foot
440 W. 5th Avenue
Chicago, Illinois
M/F Contract AF33(600)-26117

Hoffman Laboratories, Inc.
Attn: Markus McCoy
Los Angeles, California
M/F Contract AF33(600)-17529

Hughes Aircraft Corporation
Division of Hughes Tool Company
Attn: Dr. Vanatta
Florence Avenue at Teale
Culver City, California
M/F Contract AF33(600)-27615

Johns Hopkins University
Radiation Laboratory
Attn: Dr. D. D. King
1315 St. Paul Street
Baltimore 2, Maryland
M/F Contract AF33(616)-68

Fairchild Engine & Airplane Corp.
Fairchild Airplane Division
Attn: L. Fahnestock
Hagerstown, Maryland
M/F Contract AF33(038)-18499

Federal Telecommunications Lab.
Attn: Mr. A. Kandoian
500 Washington Avenue
Nutley 10, New Jersey
M/F Contract AF33(038)-13289

Glenn L. Martin Company
Attn: N. M. Voorhies
Baltimore 3, Maryland
M/F Contract AF33(600)-21703

Massachusetts Institute of Tech.
Attn: Prof. H. J. Zimmermann
Research Lab. of Electronics
Cambridge, Massachusetts
M/F Contract AF33(616)-2107

North American Aviation, Inc.
Aerophysics Laboratory
Attn: Dr. J. A. Marsh
12214 Lakewood Boulevard
Downey, California
M/F Contract AF33(038)-18319

North American Aviation, Inc.
Los Angeles International Airport
Attn: Mr. Dave Mason
Engineering Data Section
Los Angeles 45, California
M/F Contract AF33(038)-18319

Northrop Aircraft Incorporated
Attn: Northrop Library
Dept. 2135
Hawthorne, California
M/F Contract AF33(600)-22313

Ohio State Univ. Research Foundation
Attn: Dr. T. C. Tice
310 Administration Bldg.
Ohio State University
Columbus 10, Ohio
M/F Contract AF18(600)-85

DISTRIBUTION LIST (Cont.)

Commander
Air Force Missile Test Center
Patrick Air Force Base, Florida

Attn: Technical Library

Chief
BuShips, Room 3345
Department of the Navy
Attn: Mr. A. W. Andrews
Code 883
Washington 25, D. C.

Director
Naval Research Laboratory
Attn: Dr. J. I. Bohnert
Anocostia
Washington 25, D. C.

National Bureau of Standards
Department of Commerce
Attn: Dr. A. G. McNish
Washington 25, D. C.

Director
U.S. Navy Electronics Lab.
Attn: Dr. T. J. Keary
Code 230
Point Loma
San Diego 52, California

Chief of Naval Research
Department of the Navy
Attn: Mr. Harry Harrison
Code 427, Room 2604
Bldg. T-3
Washington 25, D. C.

Airborne Instruments Lab., Inc.
Attn: Dr. E. G. Fubini
Antenna Section
160 Old Country Road
Mineola, New York
M/F Contract AF33(616)-2143

Andrew Alford Consulting Engrs.
Attn: Dr. A. Alford
299 Atlantic Ave.
Boston 10, Massachusetts
M/F Contract AF33(038)-23700

Chief
Bureau of Aeronautics
Department of the Navy
Attn: W. L. May, Aer-EL-4114
Washington 25, D. C.

Chance-Vought Aircraft Division
United Aircraft Corporation
Attn: Mr. F. N. Kickerman
Thru: BuAer Representative
Dallas, Texas

Consolidated-Vultee Aircraft Corp.
Attn: Dr. W. J. Schart
San Diego Division
San Diego 12, California
M/F Contract AF33(600)-26530

Consolidated-Vultee Aircraft Corp.
Fort Worth Division
Attn: C. R. Curnutt
Fort Worth, Texas
M/F Contract AF33(038)-21117

Textron American, Inc. Div.
Dalmo Victor Company
Attn: Mr. Glen Walters
1414 El Camino Real
San Carlos, California
M/F Contract AF33(038)-30525

Dorne & Margolin
30 Sylvester Street
Westbury
Long Island, New York
M/F Contract AF33(616)-2037

Douglas Aircraft Company, Inc.
Long Beach Plant
Attn: J. C. Buckwalter
Long Beach 1, California
M/F Contract AF33(600)-25669

Electronics Research, Inc.
2300 N New York Avenue
P. O. Box 327
Evansville 4, Indiana
M/F Contract AF33(616)-2113

Land-Air Incorporated
Cheyenne Division
Attn: Mr. B.L. Michaelson
Chief Engineer
Cheyenne, Wyoming
M/F Contract AF33(600)-22964

Lockheed Aircraft Corporation
Attn: C. L. Johnson
P. O. Box 55
Burbank, California
M/F NOa(S)-52-763

McDonnell Aircraft Corporation
Attn: Engineering Library
Lambert Municipal Airport
St. Louis 21, Missouri
M/F Contract AF33(600)-8743

Michigan, University of
Aeronautical Research Center
Attn: Dr. R.D. O'Neill
Willow Run Airport
Ypsilanti, Michigan
M/F Contract AF33(038)-21573

Chief
Bureau of Ordnance
Department of the Navy
Attn: A.D. Bartelt
Washington 25, D. C.

Radioplane Company
Van Nuys, California
M/F Contract AF33(600)-23893

Raytheon Manufacturing Company
Attn: Dr. H.L. Thomas
Documents Section
Waltham 54, Massachusetts
M/F Contract AF33(038)-13677

Republic Aviation Corporation
Attn: Engineering Library
Farmingdale
Long Island, New York
M/F Contract AF33(038)-14810

Ryan Aeronautical Company
Lindbergh Drive
San Diego 12, California
M/F Contract W-33(038)-ac-21370

Sperry Gyroscope Company
Attn: Mr. B. Berkowitz
Great Neck
Long Island, New York
M/F Contract AF33(038)-14524

Temco Aircraft Corp
Attn: Antenna Design Group
Dallas, Texas
M/F Contract AF33(600)-31714